Sorption Modeling of Strontium, Plutonium, Uranium and Neptunium Adsorption on Monosodium Titanate

F. F. Fondeur
D. T. Hobbs
S. D. Fink
M. J. Barnes

May 7, 2003

Westinghouse
Savannah River Company
Aiken, SC 29808

This page intentionally left blank

Sorption Modeling of Strontium, Plutonium, Uranium and Neptunium on Monosodium Titanate

F. F. Fondeur, D. T. Hobbs, S. D. Fink, and M. J. Barnes
Waste Processing Technology Section
Savannah River Technology Center

Abstract

We examined the ability of various equilibrium isotherms to replicate the available data for the adsorption of strontium (Sr), plutonium (Pu), uranium (U) and neptunium (Np) on monosodium titanate (MST) during the treatment of simulated and actual Savannah River Site high-level waste. The data comes from numerous experimental studies conducted between 1999 and 2002. The analysis considered 29 isotherm models from the literature. As part of this study, we developed a general method for selecting the best isotherm models. The selection criteria for rating the isotherms considered the relative error in predicting the experimental data, the complexity of the mathematical expressions, the thermodynamic validity of the expressions, and statistical significance for the expressions.

The Fowler Guggenheim-Jovanovic Freundlich (FG-JF), the Fowler Guggenheim-Langmuir Freundlich (FG-LF) and the Dubinin-Astashov (DA) models each reliably predicted the actinide and strontium adsorption on MST. The first two models describe the adsorption process by single layer formation and lateral interactions between adsorbed sorbates while the Dubinin-Astashov model assumes volume filling of micropores (by osmotic pressure difference). These two mechanisms include mutually exclusive assumptions. However, we can not determine which model best represents the various adsorption mechanisms on MST. Based on our analysis, the DA model predicted the data well. The DA model assumes that an initial sorption layer forms after which networking begins in the pore spaces, filling the volume by a second mechanism. If this mechanism occurs in MST, as the experimental data suggests, then we expect all the empty and closed spaces of MST to contain actinides and strontium when saturated. Prior microstructure analyses determined that the MST surface is best described as heterogeneous (i.e., a semi-crystalline outer layer on an amorphous core) or composite material for adsorption. Therefore, we expect the empty spaces (of nanometer size) between the crystalline units in the fibrous material to provide sorption area for the actinides and strontium. Additional conclusions from this study follow.

Since each of the three models work reliably, we recommend use of the computationally simplest model as the primary tool until future work can differentiate between the two mechanisms. The Dubinin-Astashov model possesses a simpler mathematical form with fewer parameters and operations.

The experimental data for actual and simulated wastes generally showed consistent agreement. However, the data sets do include considerable variance from a number of causes including the following.

- The plutonium sorption data appears most consistent (e.g., between actual and simulated waste) and most easily predicted. Since plutonium removal efficiency proves most important for the process design efforts, this consistency of the data proves especially beneficial.
- Extremely high mass loadings of uranium on MST result in multilayer sorption behavior and divergence from classical single monolayer isotherm forms. Prior x-ray studies demonstrate that uranium begins to network, or form dimers, which agrees with this interpretation. This uranium behavior also shows a complex interaction, and a direct correlation, with sorption data for the other radionuclides. We believe this data suggests nucleation (e.g., precipitation) of the actinides in the micropore space for both neptunium and plutonium. For strontium, the high uranium loadings appear to inhibit the sorption of strontium.
- Nearly all the solutions contained uranium as the radionuclide with the highest mass concentration. This data shows the widest variance.
- The composite data set indicates a notable variance in sorption for different batches of MST. The sorption of strontium with different batches of MST shows the largest variance among the four radionuclides for different batches of MST. This variance remains a relatively unexplored aspect of the process design.
- Similarly, the experimental data included a wide variety of solution compositions. As such, the mathematical expressions implicitly account for variances in solution chemistry typical of that anticipated within the Salt Waste Processing Facility and Actinide Removal Process. The reader must consider the ranges of these concentrations when applying the expressions.
- Increasing temperature decreases strontium, plutonium and to a lesser extent uranium sorption on MST. The opposite effect occurs with neptunium. This temperature variance further suggests a nucleation behavior for neptunium.
- Nearly all the data used in developing the sorption models came from experiments using solutions with all the principle radionuclides of interest present simultaneously. We modeled the data without invoking competition between the actinides and strontium despite the large concentrations of both uranium and neptunium. Since the model does not explicitly invoke competition, the optimized parameters implicitly carry the impact of interaction within the concentration ranges of the original data. Hence, extrapolation of the models to concentrations markedly outside those ranges may result in poorer predictive ability.

This analysis suggests several key efforts needed to improve the reliability of the sorption models including the following.

- We recommend that the Salt Processing Program expand the investigation of variability for MST coming from different production batches. Testing should

also include the effect of storage (temperature and shelf-life) and pretreatment on MST adsorption capabilities.
- Additional tests should investigate Pu and Sr adsorption at Pu and Sr solution concentrations larger than 0.1 M. The recommended Pu model relies on two data points in this region that originated from one researcher.
- The program needs to assess fully the implications of increased uranium sorption of uranium on MST beyond that previously considered for nuclear criticality safety.
- The program should expand the modeling effort to consider behavior at shorter process times, such as 4 hours after addition of MST to the waste.
- We recommend studies that investigate adsorptions of single actinide and two actinides in solution at a time. This testing will validate the values of the parameters obtained in the multi-component tests and will also explore the nature of the complex interaction (e.g., between uranium and neptunium) observed at high mass loadings.
- We recommend collecting additional data for americium and curium adsorption from testing.

Introduction

The Salt Waste Processing Facility at Savannah River Site (SRS) includes adsorption as a unit operation for removing traces of alpha and beta-emitting elements from the waste solution. The facility uses monosodium titanate for Sr and actinide removal. In particular, the objective of the process is the removal of strontium (90), plutonium (238 and 239), and neptunium (237) with MST. To this end, personnel conducted a number of batch contacting experiments to obtain information related to the kinetics and capacity of the media. The tests demonstrated the ability of MST to remove both Sr and the actinides from alkaline solutions containing up to 90,000 times as much sodium as sorbate (on a molar basis).

These successful performance tests identified the need for additional scientific work to understand the interaction between the actinides and MST. Recently, SRTC personnel conducted X-ray scattering experiments such as EXAFS (Extended X-rays Adsorption Fine Structure) and TEM (Transmission Electron Microscopy) on MST.[1,2,3] The analysis indicated MST is an amorphous, spherical particle (with average diameter of about 4-5 microns) coated with about 150-500 nanometers of a crystalline and fibrous material. The fibrous material contains distorted titanium oxide octahedra. An EDS (Energy Dispersive Spectrometry in a TEM) scan of the fibrous layer of strontium-loaded MST indicated that Sr tends to adsorb on the fibrous layer of MST. The studies could not definitively identify the physical location of the actinides within the microstructure due to the low detection limits for these elements and their lower relative concentrations. The structural studies identified the differing nature of the surface chemistry for the various radionuclides. These findings include the following.

- Presence of Ti in the second coordination shell of the Sr^{2+} on the MST suggests that specific adsorption is the predominant mechanism and that electrostatic bonding (also

known as ion exchange of hydrated surface-associated species such as dissolved Na^+) in the electric double-layer of the HLW salt simulant solution does not occur.

- Uranium(VI) sorbs via an inner sphere/specific adsorption mechanism as predominantly dimeric nitrato or carbonato complexes of U(VI) species via bidentate linkages (i.e., assuming the presence of Ti octahedra in the MST structure, the U(VI) is bound to Ti groups at two different U-Ti radial distances) at high loadings. Monomeric species predominate at low loadings.
- Plutonium, added as Pu(IV), exhibits inner sphere/specific adsorption as polymeric (colloidal) Pu species—with a local environment that is consistent with Pu(IV).
- Neptunium, from salt solutions spiked with a Np(V) stock solution, exhibits inner sphere specific adsorption as polymeric Np species. The Np may be present as Np(V) or Np(IV).

From the above spectroscopy and scattering work conclusions, the actinides of interest and strontium bind specifically to MST. Therefore, we can neglect non-specific or electrostatic adsorption as described by the Diffuse Double Layer, Triple Layer, Capacitance Layer, Debye-Huckel, and Donnan Theories. This work focused only on specific adsorption as described by isotherms.

For successful implementation of MST, the adsorption process needs to use an optimal amount of MST and must remain predictable under plant-upset conditions. These recent studies provide, for the first time, sufficient data to derive a model for predicting such performance.

Adsorption is a general term that refers to the disappearance of solutes from solutions with the presumption of adsorption to a solid surface. The accumulation of solutes at the solid-liquid interface results from physical or chemical interactions with the surface. Physical bonding is relatively weak while chemical bonding is a stronger interaction which may involve ionic or covalent bonding (in addition to van der Waals and London forces). The nature of both the solid surface and the solute determines the interaction.

Inorganic surfaces consist of mostly oxygen and hydroxides. In high pH (very caustic solutions), the inorganic surfaces are mainly oxygen anions. Exchangeable cations (e.g., alkali metals such as Li and Na) are assumed to be fully hydrated and may completely shed their waters when sorbing on the surface (due to weak interaction with the surface). Cations such as K^+ and Cs^+ completely dehydrate during sorption and form strong ionic bonds with the surface. In caustic solutions, alkaline earth metals such as strontium do not fully hydrate ($Sr\text{-}OH^+$). Therefore, a strong (ionic) interaction with inorganic surfaces is expected. In contrast, anions are expected to strongly sorb on solid surfaces. The adsorption of anions is believed to occur via displacement of surface hydroxyls and the formation of mono and bidentate surface complexes with covalent bonding character. In SRS supernate, uranium and plutonium exist as anion complexes of hydroxyls, carbonates and nitrates. The hydroxyls in the complex can be displaced and covalent bond formation with the surface oxygen is expected.

To predict and scale-up adsorption operations, personnel require a detailed knowledge (including mathematical relationships) of the adsorption process of the nuclides on MST. They require a mathematical relationship describing distribution of the nuclides between the waste and the sorbent (e.g., isotherms). Numerous such models exist based on both thermodynamics and empirical regression.

If the adsorption increases proportionally to the solute concentration, the adsorption process follows Hooke's law. If the adsorption reaches a steady state value regardless of the solute concentration, then one can mathematically describe the adsorption process with a Langmuir equation.[4,5] For systems that exhibit nonlinear increases in adsorption with solute concentration, several mathematical formulas can describe the adsorption process. Examples of nonlinear isotherms include Freundlich,[6] Dubinin-Ashtakov,[7,8,9] Tempkin,[10] Volmer,[11] Sips,[12] Fowler-Guggenheim,[13,14] Frumkin-Damskin,[15] Redlich-Peterson,[16] Toth,[17] Levan-Vermeulen,[18] Vacancy Solute Theory,[19] Radke-Prausnitz,[20] Sigmoidal,[21] General Adsorption Theory,[22] Langmuir-Freundlich,[23] Margules, Fowler-Guggenheim/Langmuir-Freundlich,[24] Fowler-Guggenheim/Jovanovic-Freundlich,[25] Jaroniec,[26,24] Ideal Adsorbed Solute Theory,[27,28,29] and Sheindorf-Rebuhn-Sheintuch[30] (see Appendix A). It is important to note that successfully fitting isotherms to adsorption data does not, in general, provide information about the mechanism of sorption. These expressions are best looked at as mathematical descriptors of the sorption data. However, the mathematical relations are useful for predicting and scaling adsorption operations. Personnel must derive mechanistic details of sorption processes from other techniques such as surface spectroscopy (infrared, Raman, EXAFS, etc.).

We numerically optimized the parameters for the various published isotherms to available actinide and strontium adsorption data for sorption onto MST. We attempted to identify the best isotherm model that fit available data and reliably predicted MST performance as a function of MST and sorbate concentrations.

Experimental Data: Simulated and Actual Waste

We obtained the actinide and strontium data for simulated waste from previous research efforts and compiled the information into one data set.[31,32,33,34] These experiments used the same basic protocols for studying the removal efficiency of MST. Personnel kept a slurry of MST and simulated waste at constant temperature. Most data comes from work at ambient temperature (e.g., 25 °C) although a few experiments examined performance at elevated temperatures (i.e., 45 and 65 °C). Tests most typically used solutions containing uranium, strontium, plutonium, and neptunium in combination. Table 1 shows the range of concentrations studies. The experiments also examined removal performance as a function of solution composition and, to a more limited extent, for different manufacturing lots of MST. Table 2 shows the range of solution compositions included in the studies.

Table 1. Initial sorbate concentrations.

	Concentration (μg/L)			
Dataset	Sr	Pu	Np	U
Phase III[31]	5 – 100	1.1 – 280	340 – 36000	1500 - 26000
Phase IV[32]	90	62	420	9000
Phase V[33]	87	190	420	9000
Alternate Matls[34]	65 - 100	98 - 220	460 - 650	10000 - 12000
Soln Comp[34]	300 - 830	36 - 240	190 – 310	4300 - 10000

Table 2. Experimental compositions.

Dataset	MST (g/L)	Sorbate Equiv (μmole/L)	OH^- (M)	NO_3^- (M)	Na+ (M)
Phase III[31]	0.2, 1.1, 2.0	13 – 380	1.1 -1.8	2.1 – 3.5	4.5 – 7.5
Phase IV[32]	0.2, 0.4	51 - 99	2.4	1.1	4.5
Phase V[33]	0.2, 0.4	84	1.3	2.6	5.6
Alternate Matls[34]	0.4	92 – 110	2.6	1.3	5.6
Soln Comp[34]	0.4	51 – 110	1 – 3	1 – 3	4.8 – 5.9

The bottles were shaken in a temperature-controlled bath for finite length of times. At the end of the shaking, personnel filtered the solutions and analyzed the filtrate using Inductively Coupled Plasma Mass and Emission Spectroscopy as well as analyzing for plutonium by PuTTA separation and radiocounting. Personnel assumed the loaded amount of actinide and strontium on MST equaled the difference between the original concentration in stock solutions and the final concentration in the bottles. The amount of uncertainty reached 10 to 15% CV (Coefficient of Variation, or percent uncertainty). The error associated with weighting MST equaled 5%. Propagation of errors calculation places the uncertainty in the actinide and strontium loading between 5 and 10% CV.

The experimental data for actual and simulated wastes generally showed consistent agreement. However, the data sets do include considerable variance from a number of causes including the following.

- Extremely high mass or molar loadings of uranium on MST result in multilayer sorption behavior and a unique divergence from classical single monolayer isotherm forms.
- Nearly all the solutions contained uranium as the radionuclide with the highest mass concentration. The uranium data shows the widest variance.
- The composite data set indicates a notable variance in sorption for different batches of MST. The sorption of strontium with different batches of MST shows the largest variance. This variance remains a relative unexplored aspect of the process design.

Further examination of the experimental data set identified additional data points measured at the detection limits of measuring instruments. The large variance of the data measured at detection levels places great uncertainty on the data in the isotherm. We eliminated data points measured at the detection limit from additional calculations. In the case of the Pu experimental points, only 60 out of 110 data points remained above detection limits. Further, we imposed an additional screening criterion on the maximum radionuclide (i.e., sum of all four species) loading on MST allowed. The amount of sorbate should not exceed 2 umole/g of MST. This criterion is based on the maximum expected number of equivalence MST can absorb by analogy with typical sorbents.[35] Appendix B lists the Pu, Np, U and Sr experimental data.

Similarly, the experimental data included a wide variety of solution compositions. As such, the mathematical expressions implicitly account for variances in solution chemistry typical of that anticipated within the Salt Waste Processing Facility and Actinide Removal Process. The reader must consider the ranges of these concentrations when applying the expressions.

Model Selection

The fitting of experimental data to complex multi-component models requires a number of decisions on approach, some of which are subjective. We adopted two strategies for modeling the data. For each model we decided to fit all of the data simultaneously. Our

second strategy constrained the parameter with the largest standard deviation. Large parameter deviations are typically due to limitations of the experimental design, the restricted size of the datasets, or an insufficient span of the data.

We evaluated the data for steady state (i.e., after 168 hours) and mass balance consistency. We identified 29 different isotherm models (see Appendix A) for fitting to the data using JMP® software (version 5.0.1 from SAS Institute). The modeling generated correlation coefficients, sum of the squares of error values (variance), "lack of fit" and significance probabilities for each isotherm. We used each of these criteria to rank the isotherms. In addition, we used Akaike's number to define a mathematical "simplicity factor" for the expression. The Akaike number is given by[36]

$$n\log(SSE)+\frac{2n(p+1)}{(n-p-2)}$$

where n is the number of data points, p is the number of parameters in the model and SSE is the sum of the squares of the errors. An Akaike number closer to zero indicates a simpler mathematical expression. As a final criterion, we gave preference to those isotherms that provide a thermodynamically consistent representation of the data. In principle, such expressions hold a higher likelihood of extrapolating beyond the region of the original data used to obtain the parameters.

We ranked each isotherm expression separately for the performance relative to uranium, plutonium, strontium, and neptunium. We summed the individual rankings, with equal weightings, for each criterion for each radionuclide. Tables C1 to C4 (in Appendix C) provide the rankings for the various radionuclides.

An objective of this evaluation is the selection of one isotherm that can fit all four sorbates. The result of the fittings resides in laboratory notebook WSRC-NB-97-62. We included, in this modeling effort, 110 data points from the simulated waste tests and 27 data points from the actual waste tests. As mentioned earlier, we omitted data points that lacked mass balance consistency, that fell below the detection limit for a given radionuclide, or when the sum of masses for all the radionuclide exceeded our understanding of the available sorption sites on MST. The resulting number of data considered for Sr included 95 data points, for U 110 data points, for Pu 68 data points, and for Np 82 data points.

Results and Discussion

Simulated and Actual Waste Modeling (Equilibrium Data)

We found three isotherms that reproduced the data in reasonably good fashion: the Fowler-Guggenheim-Jovanovich-Freundlich (FG-JF), Fowler-Guggenheim-Langmuir-Freundlich (FG-LF) and the Dubinin-Astashov isotherms. The Dubinin-Astashov model performed best per the selection criteria we defined. All three models replicated the non-classical sorption behavior observed for uranium at extremely high mass loading

resulting in an "upswing" in the curve associated with multi-layer sorption behavior. Other models could not both incorporate this behavior and simultaneously replicate data at lower mass loadings with practical error, or offset, from the experimental data. The FG-JF and FG-LF isotherms assume interactions between the adsorbed sorbates, between the solution and surface sorbates and exponentially distributed surface energy sites on MST. The inclusion of many assumptions requires calculation of several parameters. On the other hand, the DA isotherm assumes an inverse Weibull distributed surface energy sites on MST. The DA isotherm requires only four parameters to represent sorbate loading. We provide results from the FG-JF (in Appendix C) and DA isotherms (below) in this paper. A brief introduction to inverse Weibull distributions follows.

The inverse Weibull distribution function is a two parameter function. The mathematical form of this function follows.

1) $F(x) = e^{-(S \times X)^n}$

In this expression, "S" and "n" are the scale and shape parameter. The parameter "x" is the random variable and in this case is the sites energy on MST. This function is unimodal with a maximum ($e^{-(1+1/n)}$) at a "x" value of $S(1+1/n)^{-1/n}$. Increasing the value of "n" increases the width at half maximum of the distribution. Figure 1 shows the effect of the parameter "n" on an inverse Weibull distribution with a maximum near the origin.

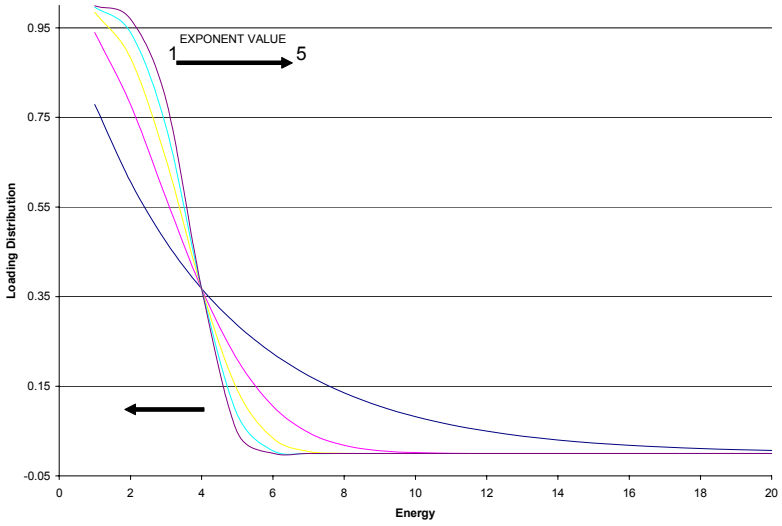

Figure 1. The effect of the exponential parameter of the distribution shape of an inverse Weibull.

The Dubinin-Astashov model incorporates this energy distribution as follows.

$$Y = Y_m \exp\left[-\left(\frac{RT}{E}\right)^n \left(Ln\left(\frac{S}{X}\right)\right)^n\right]$$

In this model, E represents the average adsorption energy. The parameter "S"represents the saturation limit of the radionuclide. The value Y_m represents the maximum radionuclide loading on MST.

We used a number of isotherm models to regress the plutonium adsorption data. Table 3 lists the fitting results of the isotherm models. Not all the isotherms successfully reproduced the data and we omit from the table those isotherms that failed to converge for the data set. Table 3 also includes the overall performance of each model. The performance evaluation listed in Table 3 includes calculated results and statistical significance. We base our selection of the Dubinin-Astashov model on the overall ranking using the criteria defined earlier (e.g., correlation coefficients, sum of the squares of error values (variance), "lack of fit" and significance probabilities for each isotherm, and the mathematical "simplicity factor).

None of the ideal behavior isotherms such as Langmuir or the Ideal Adsorbed Solute theory (IAST) or Freundlich performed well. The FG-JF and FG-LF models are mathematical combinations of the Fowler-Guggenheim, Langmuir, Jovanovic and Freundlich isotherms. These models include the interactions between loaded sorbents, between the loaded and free sorbate and surface heterogeneity. The successful prediction of the Pu, Sr, U and Np data with the FG-JF and FG-LF models may indicate appreciable sorbate interactions and surface heterogeneity. On the other hand, the Dubinin-Astashov (DA) model successfully reproduced this data. The DA model is based on the thermodynamic potential for adsorption (Gibbs energy) on sites with energies distribution described by a Weibull function. The DA isotherm successfully models filling of micropore spaces that occurs subsequent to the initial sorption layers. The DA model does not include loaded sorbate-to-sorbate interactions terms but has successfully fitted multi-layer adsorption data. The successful fitting with the DA model reinforced the view of a heterogeneous MST surface. Since two different types of models (FG-JF or FG-LF and DA) successfully reproduced the data, we chose the model with the least number of variables and mathematical operations. Models with complex mathematical operations and numerous parameters exhibit large sensitivity to small variations. We recommend the DA model for further engineering calculations.

We fitted the Pu adsorption data at 25 ºC. Figure 2 shows the DA isotherm for the 25 ºC results. Most of the data shown on Figure 2 derives from simulant testing. The two data points at concentrations larger than 0.55 µM (i.e., 1757 nCi/g of ^{238}Pu or 6.4 nCi/g of ^{239}Pu) derived from actual waste testing. The actual waste data came from testing under non-steady state conditions (i.e., after only 24 hours of sorption testing). Glancing at Figure 2, the DA model successfully explained 72% of the variance ($R^2 = 0.72$) in the Pu adsorption data. Note the relatively large data scatter at plutonium concentrations less than 0.1 µM. The scatter represents the collection at several different experimental conditions. To ensure accurate calculation of the parameters in the model, the data must include the initial rise and plateau (i.e., saturation) of the loading-final concentration curve. Figure 2 shows a large compilation of data at the initial rise of the curve and only two points at the plateau of the curve. The two data points at a plutonium concentration

of 0.55 (i.e., 1757 nCi/g of ^{238}Pu or 6.4 nCi/g of ^{239}Pu) and 0.7 µM (i.e., 2236 nCi/g of ^{238}Pu or 8.14 nCi/g of ^{239}Pu) originated from one adsorption experiment terminated 24 hours after initiation of sorption testing. Therefore, the proposed calculated parameters depend heavily upon the accuracy of these two data points. The additional two dashed-line curves are the 95% prediction confidence curves. The predictions curves agree well at low Pu concentrations and diverge widely at high Pu concentrations. The large variance in the 45 and 65 ºC data resulted in a poor fitting with the DA model. In general, the amount of Pu loaded on MST at 45 and 65 ºC proved lower than at 25 ºC.

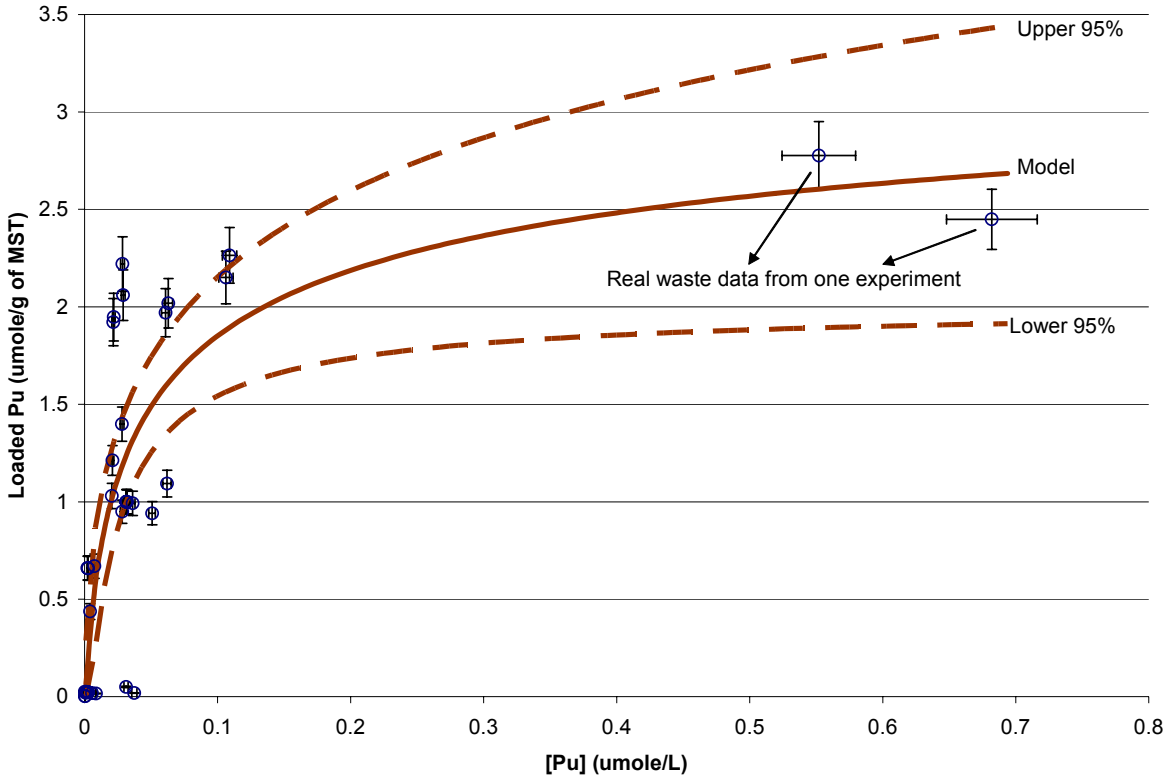

Figure 2. The prediction of the Pu data with the Dubinin-Astashov model. (NOTE: The data shown comes from experiments at 25 ºC.). The two data points above 0.55 µM are actual waste data. The waste data results from testing under unsteady state conditions (i.e., only 24 hours of testing).

Table 3. Relative performance of models for plutonium and overall.

Model	Plutonium r^2	Plutonium Akiake	Overall Score	Overall Ranking
Competitive Quadratic with U	0.752	71	15	6
Dubinin-Astashov	**0.72**	**66**	**5**	**1**
Langmuir	0.69	69	12	5
Radke-Prausnitz	0.69	69	10	4
Langmuir Uniform Distribution	0.69	69	9	3
Khan	0.69	69	8	2
Langmuir-Freundlich	0.687	69	17	8
BET	0.687	69	17	8
Toth	0.687	69	15	6
General-Y	0.685	-104	30	14
Jaroniec-Marczweski	0.679	72	27	13
Bubinin-Radushevik	0.679	70	23	11
Redlich-Peterson	0.679	70	23	11
SRS	0.678	68	18	10
FG-LF	**0.67**	**-105**	**36**	**17**
Myers	0.617	-104	35	16
Volmer	0.616	-106	39	20
IAST	0.616	-106	39	20
Jovanovic	0.616	72	32	15
FG-JF	**0.585**	**-99**	**38**	**18**
Temkin	0.46	81	38	18

Plutonium Form of the Dubinin-Astashov Model

The DA equation for Pu loading on MST at 25 ºC follows.

$$2)\quad Loaded\ Pu = (2.6 \pm 0.5) \times \exp\left(-8 \pm 6 \times 10^{-4} \times Temperature^{2\pm1} \times \left[Ln\left(\frac{0.8 \pm 1.2}{[Pu]} \right) \right]^{2\pm1} \right)$$

In this expression, the temperature is in units of Kelvin and the plutonium concentration unit is in micromoles per liter. Note the value of the exponent for both the concentration and temperature equals 2. A value of 3 or less is typically assigned to a narrow energy distribution for sorption sites. The surface homogeneity assumed from the DA model is not consistent with previous microscopy and spectroscopy analysis of MST. The value 0.0008 (which equals the "a" parameter) equals to the gas constant divided by the average adsorption energy (R/E) raised to the "nth" power and in this the 2nd power. From this expression we can calculated the average adsorption energy "E". The calculated average adsorption energy from the previous expression equals 294 J/mole. This energy is well below the adsorption energy of strontium on clay (typically 7 kJ/mole).[37] The low sorption energy value explains the ease of actinide sorption on MST. The energy of ion exchange reactions typically ranges from 8-16 kJ/mol. The calculated energy value of 294 J/mole indicates the mode of adsorption is specific (or multilayer), in agreement with recent XAFS findings.

We fitted the three temperature data sets simultaneously with the DA function. The DA model explained 74% of the variance in the data. The Dubinin-Astashov equation for Pu loading on MST follows.

$$3)\quad Loaded\ Pu = (471 \pm 174) \times \exp\left(-.27 \pm .14 \times Temperature^{0.4\pm.02} \times \left[Ln\left(\frac{3.6 \pm 9}{[Pu]} \right) \right]^{0.4\pm.02} \right)$$

In this expression, the larger parameter uncertainty is due to additional data scatter from the wider temperature range tested. The parameter listed before the temperature variable and the parameter in the logarithm term may not be statistically significant.

Figure 3 shows the effect of temperature on Pu adsorption. There are two curves on Figure 3. The leftmost curve is the temperature dependence of the Pu loading as predicted by the DA model. The model predicts loading decreases with increasing temperature. Raising the temperature during sorption provides additional thermal energy for the loaded Pu to desorb. Please note testing included only three temperatures. The right curve on Figure 3 is the DA isotherm model prediction of loading and final Pu concentration at 45 ºC. Note the linear dependency between loaded Pu and temperature indicates the isotherm shape does not change with temperature. The isotherm linearly shifts to lower values at high temperatures (within the range tested).

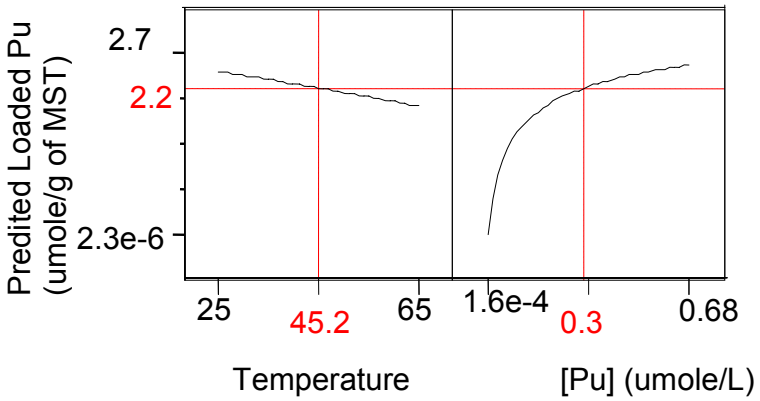

Figure 3. The effect of temperature on Pu adsorption as predicted by the Dubinin-Astashov model.

Regression of the data for the plutonium loading equation resulted in a significant uncertainty in the parameter values. For example the uncertainty of the "S" parameter is three times larger than the estimated value. The "S" (previously identified as the shape factor for a Weibull distribution) parameter stands for the solubility limit of the nuclide in solution. To determine how sensitive the DA equation is to parameters variations, we computed and graphed the sensitivity factors. Figure D1 in Appendix D contains the sensitivity plots.

Strontium Form of the Dubinin-Astashov Model

Figure 4 shows the loading data as well as the DA model prediction for strontium sorption at 25 ºC. Again, the large variance of the 45 and 65 ºC precluded fitting with the DA model at these two temperatures alone. The DA model explained 97% of the data variability ($R^2 = 0.97$). The data scatter at [Sr] <0.1M is due to different experimental conditions tested in the adsorption experiments. The DA model reproduced this scatter by including the effects of temperature. In Figure 4, the points represented by the filled circles are DA model predictions. The final DA isotherm equation presents a heterogeneity value ("n") of 1. The site energy distribution is very narrow. The surface of MST appears very homogeneous for Sr adsorption. The average adsorption energy, as predicted by the DA model, is 3.3 kJ/mole. This enthalpic energy is above the energy available at room temperature (2477 J/mole) for Brownian motion. Therefore, the strontium sorption is irreversible. The inverse Weibull statistics indicate that, to maximize the specific loading, the energy must be as large as possible. Also from the DA equation, the maximum Sr loading on MST is predicted to be 31 micromoles per gram of MST (e.g., the pre-exponential term in the following equation) at a 95% confidence level. No experimental measurement of the maximum Sr loading on MST has been made to date for comparison. To convert from µmol/L of Sr-90 to nCi/g of solution multiply the µmol/L unit by 9960 (assuming a solution density of 1274 g/L).

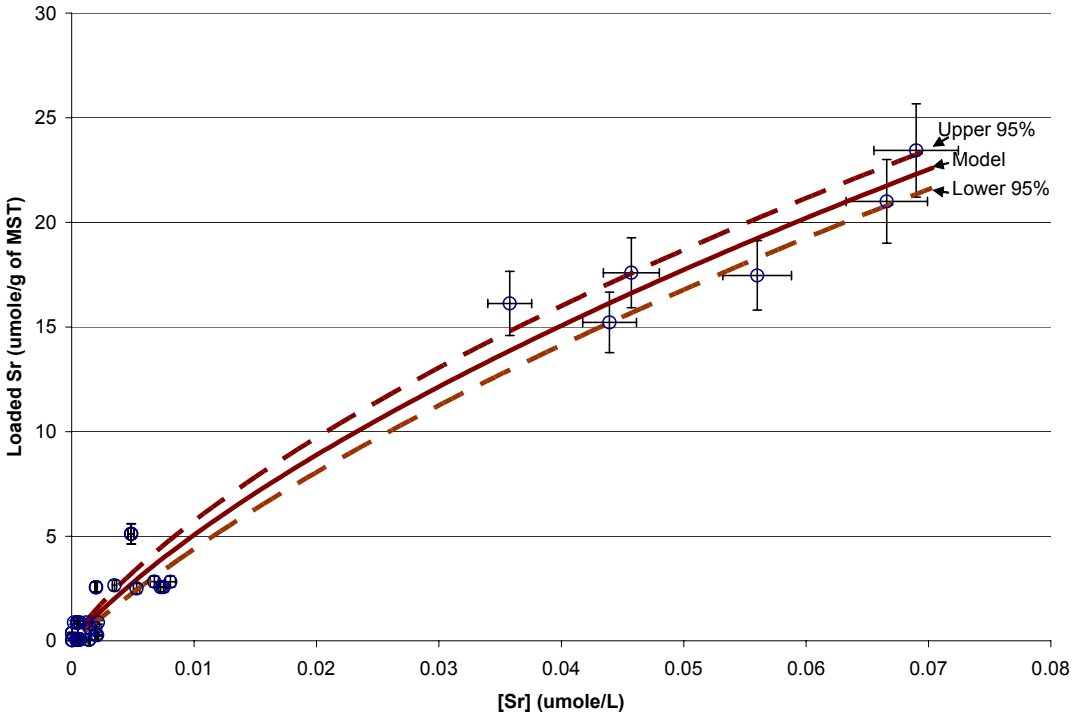

Figure 4. The Dubinin-Astashov model predictions for the Sr loading data at 25 ºC. The confidence limits are for the mean response. Please note the error bars on the data.

The corresponding DA equation for strontium at 25 ºC follows. The "±" terms in the equations represent the standard error for the parameters.

$$4)\quad Loaded\ Sr = 22 \pm 19 \times \exp\left[-2.3 \pm 0.9 \times 10^{-3} \times 298^{1\pm.33} \times \left(Ln\left(\frac{0.07 \pm .12}{[Sr]} \right) \right)^{1\pm.33} \right]$$

The pre-exponential and the logarithm parameters may not be statistically significantly since they have strong correlations with the other parameters. We also fitted the data for all three temperatures simultaneously yielding the following equation. The Dubinin-Astashov model equation for Sr loading follows with the same units as used for plutonium.

$$5)\quad Loaded\ Sr = 410 \pm 138 \times \exp\left[-0.09 \pm 0.02 \times Temperature^{0.55\pm.009} \times \left(Ln\left(\frac{0.42 \pm .12}{[Sr]} \right) \right)^{0.55\pm.009} \right]$$

Note at 298 °K both equation 4 and 5 predictions differ suggesting additional work is needed. We recommend equation 5 for strontium loading predictions. The effect of

temperature is shown in Figure 5. Looking at Figure 5, the DA model predicts that increasing the temperature decreases Sr loading on MST. Raising the temperature during sorption provides additional thermal energy for the loaded Sr to desorb. The sensitivity plots for this equation are shown in Appendix D.

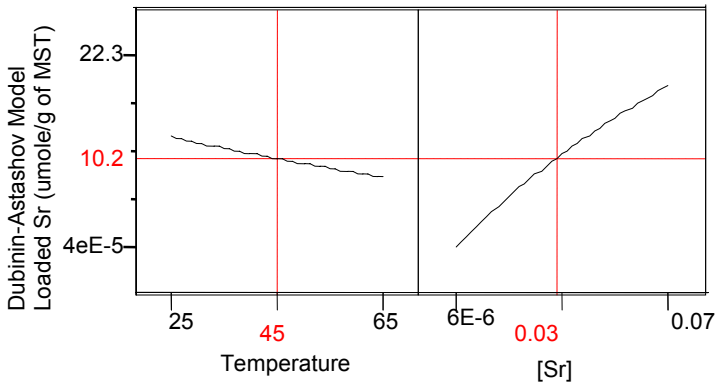

Figure 5. The effect of temperature on Sr adsorption as predicted by the Dubinin-Astashov model.

Uranium form of the Dubinin-Astashov Model

Figure 6 shows the experimental loading data as well as the DA model predictions at 25 ºC. Figures 7 and 8 show similar predictions for the 45 and 65 °C data. Figure 9 shows the results for the DA model with parameters regressed simultaneously for the entire data set. The loading data display a take off or "tail" at [U] > 65 micromoles/L. This likely indicates multilayer formation as originally suggested by previous scattering spectroscopy work. The feature of the DA model in reproducing the upper "tail", or "upswing", suggests formation of chemical networks throughout the micropore space. If the DA model assumptions are correct, then the sites energy distribution on MST is very narrow and homogeneous (as indicated by the "n" value of 0.16).

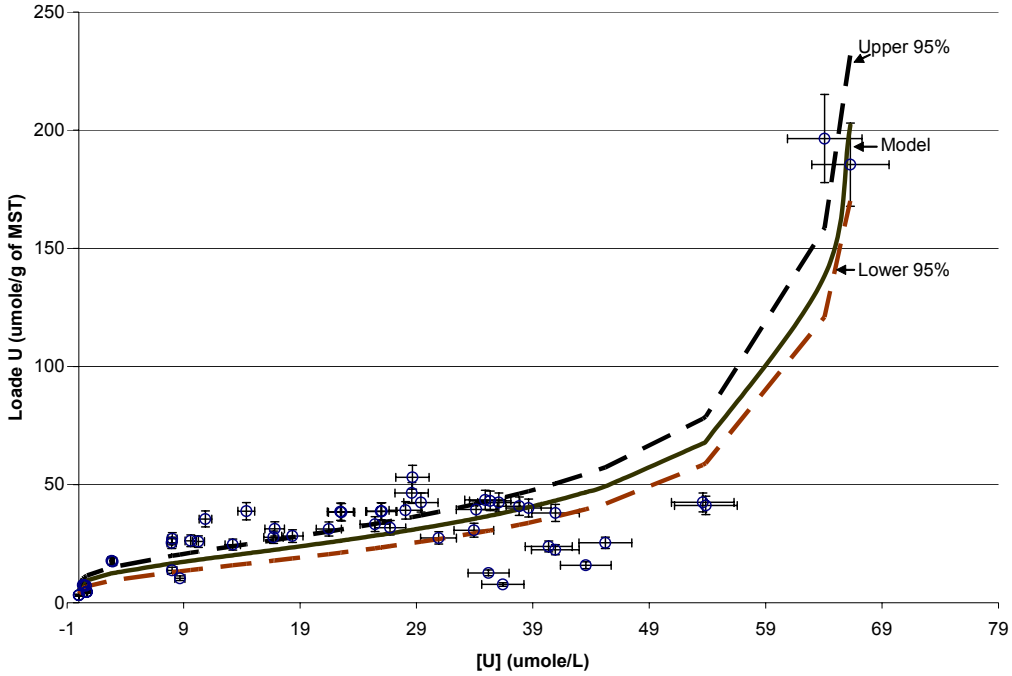

Figure 6. The Dubinin-Astashov model fit of the U data at 25 ºC.

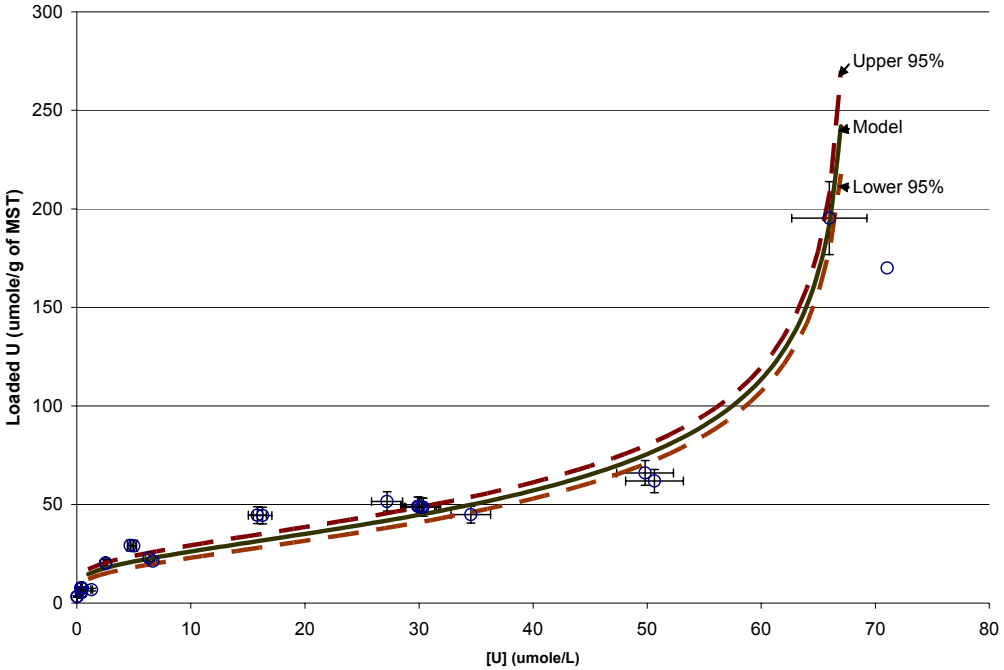

Figure 7. The Dubinin-Astashov model results and the 45 ºC U adsorption data.

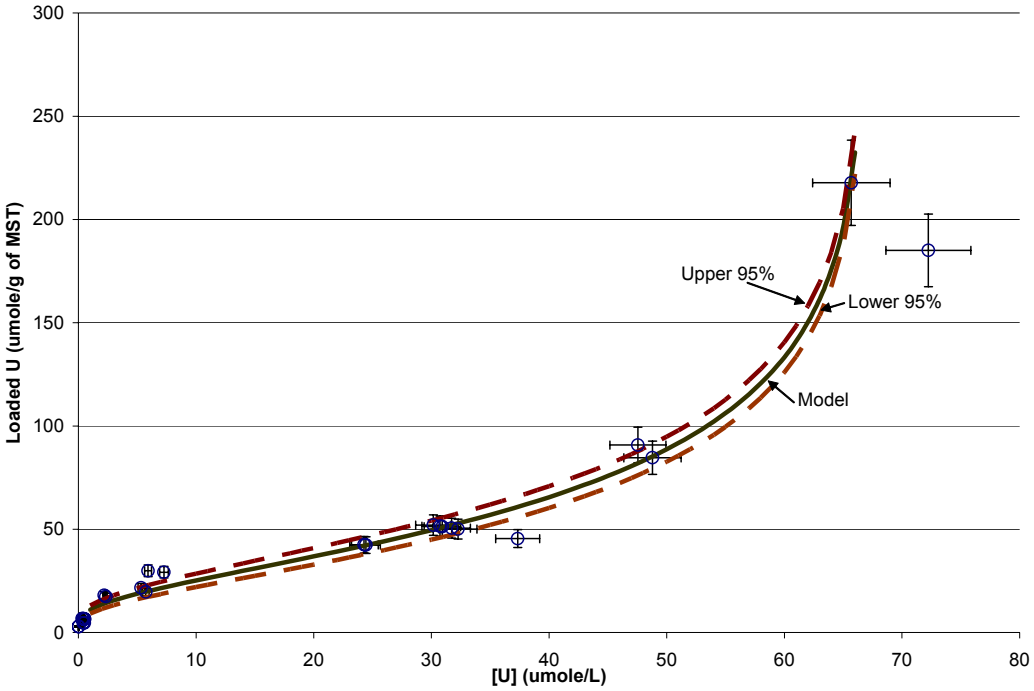

Figure 8. The Dubinin-Astashov model output for the 65 ºC uranium data.

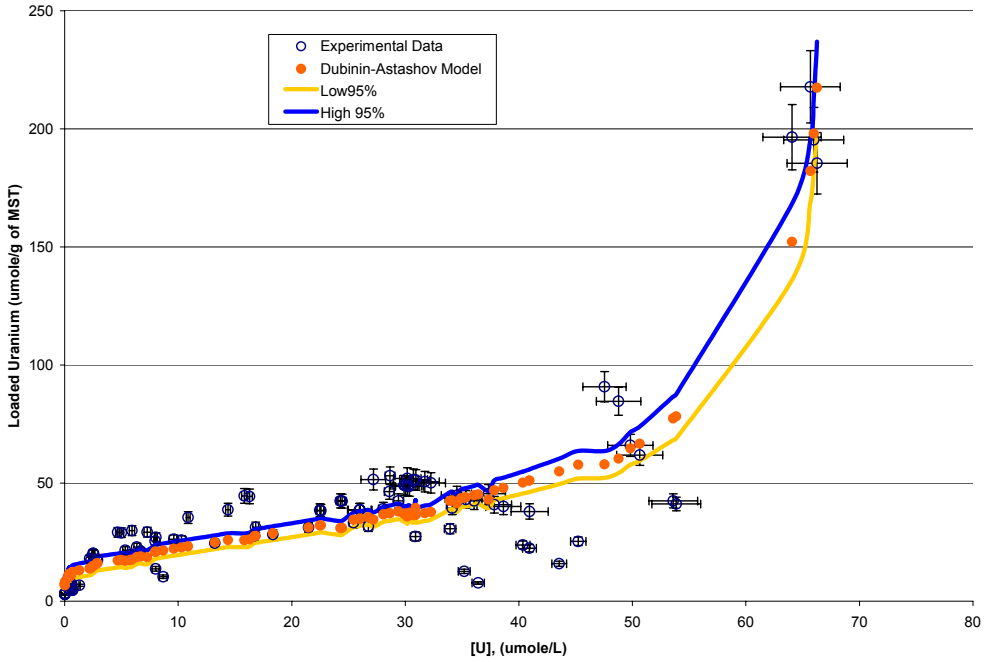

Figure 9. The Uranium loading data on MST at 25, 45 and 65 ºC. The figure also includes the Dubinin-Astashov model predictions.

The average adsorption energy on MST is very low, about 5 J/mole. The magnitude of this energy indicates multilayer formation. This low sorption energy explains the irreversibility of the adsorption process (for example low leaching under washing conditions). Note the parameter listed before the temperature variable in Eq. 6 may not be statistically significant. Figure 10 shows the effect of temperature on the predictions. From inspection of Figure 10 temperature has a minor effect on uranium loading. The DA model predicts MST can adsorb 1,865 micromoles of uranium per gram of MST (or 44 wt%). The previously experimentally determined maximum loading is 1.28 wt %.[32] The predicted maximum loading is 34 times the experimental value. We recommend additional testing at large uranium concentrations (> 100 umole/L) to accurately determine the maximum capacity of MST for fissile uranium. This information is essential for developing the safety bases for the operations.

The Dubinin-Astashov isotherm equation for U loading follows using the same units as stated earlier.

$$6)\ \ Loaded\ Uranium = 1865 \pm 472 \times \exp\left[-20 \pm 15 \times Temperature^{0.16 \pm .008} \times \left(Ln\left(\frac{68 \pm 0.3}{[U]} \right) \right)^{0.16 \pm 0.008} \right]$$

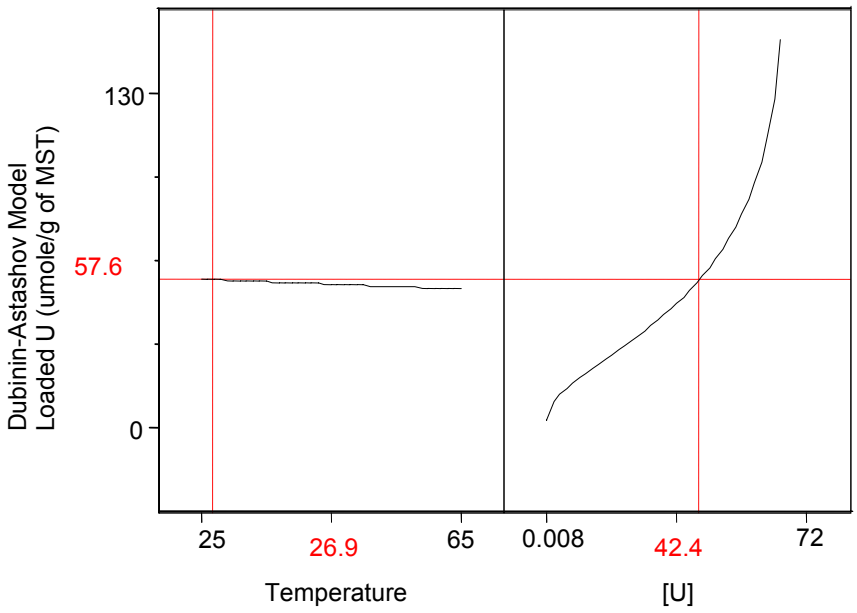

Figure 10. The effect of temperature on U adsorption as predicted by the Dubinin-Astashov model.

Neptunium Form of the Dubinin-Astashov Model

We organized the Np data according to temperature and plot it in Figure 11. Inspection of data in Figure 11 shows that higher adsorption occurred at higher temperature. This observation is contrary to the temperature dependency of U, Pu and Sr. At each temperature, we fitted the DA model to the data. Figures 12, 13 and 14 shows the Np adsorption data and DA predictions. The Dubinin-Astashov equation for the Np sorption data at 25ºC follows.

$$Loaded\ Np = 64.9 \pm 9 \times \exp\left[-0.001 \pm .0006 \times 298^{1.1 \pm .5} \left(Ln\left(\frac{75.3 \pm .01}{[Np]} \right) \right)^{1.1 \pm .5} \right]$$

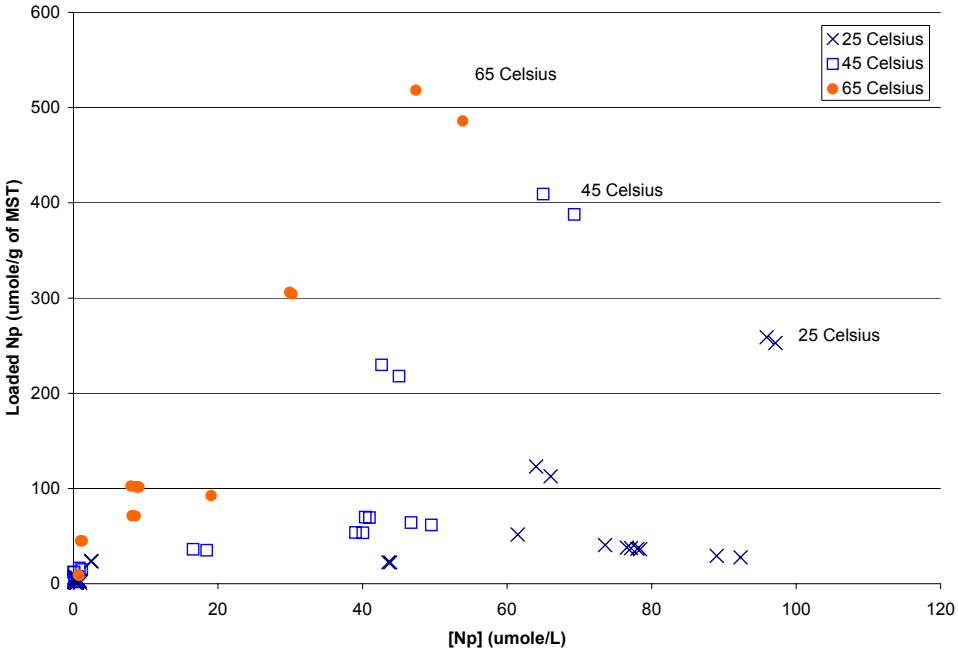

Figure 11. The Np adsorption data as a function of temperature.

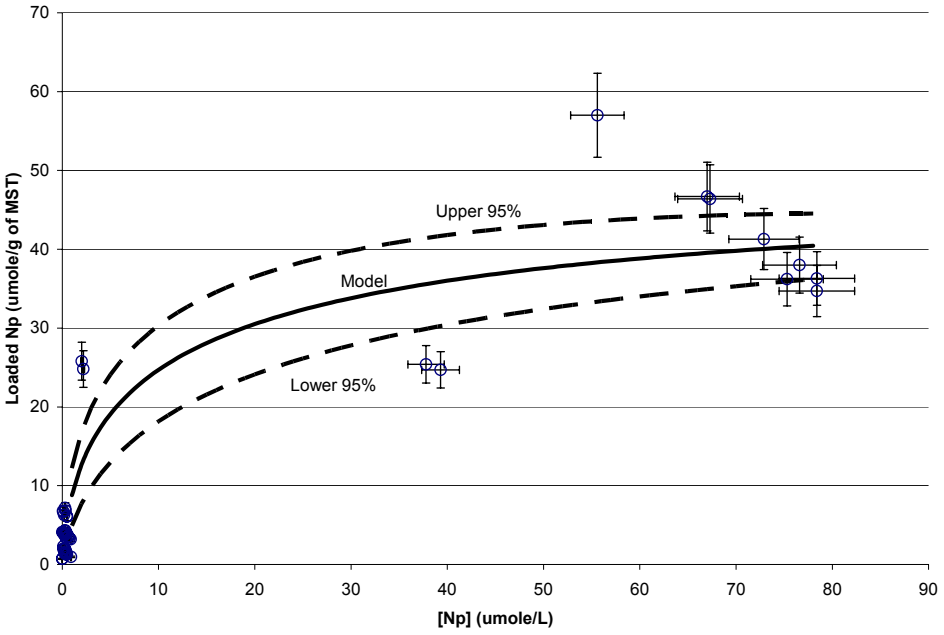

Figure 12. This figure shows the Np adsorption data at 25 ºC and the Dubinin-Astashov model predictions. Please note some of the high loading data are not shown.

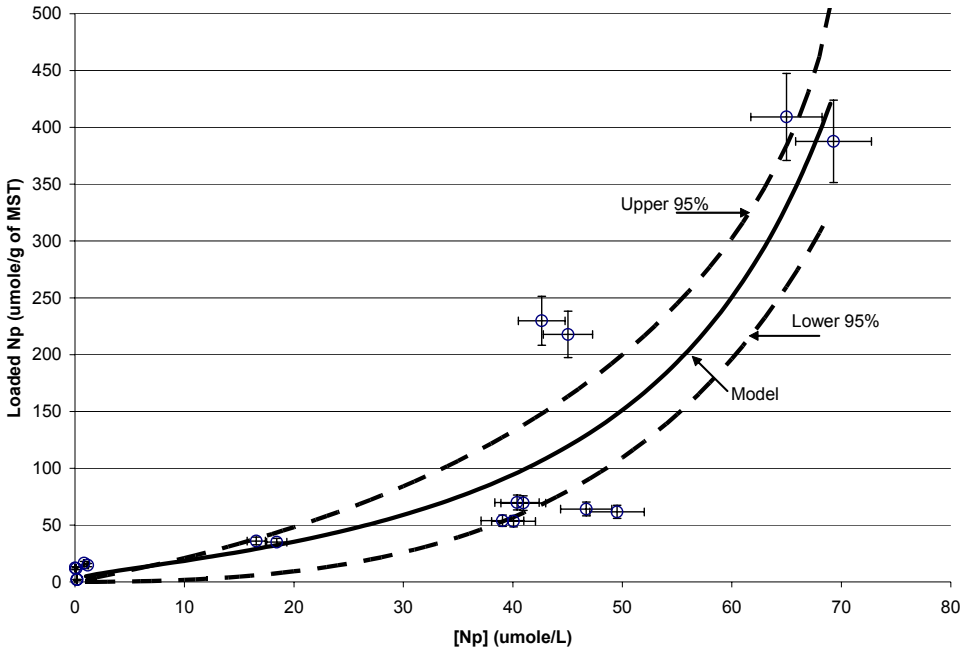

Figure 13. The Np sorption data at 45 ºC and predications by the Dubinin-Astashov model.

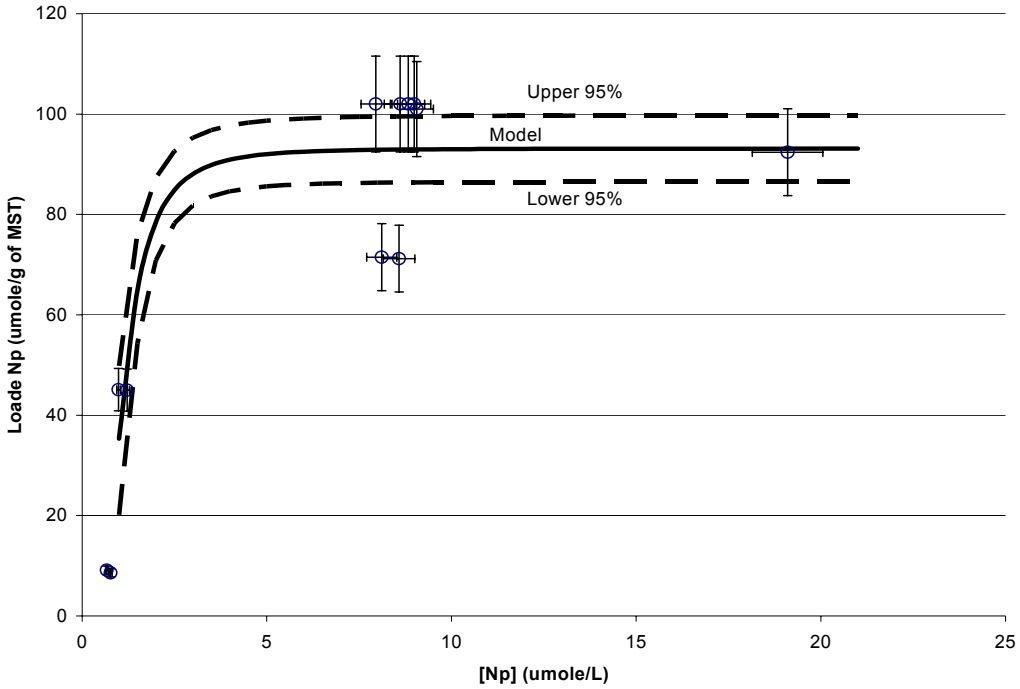

Figure 14. The 65 ºC Np data fitted with the Dubinin-Astashov model.

Sorption Data After 24 hours of Testing

The U, Np, Sr and Pu sorption Figures after 24 hours are shown in Appendix E.

The Effect of Excess Uranium Loading on Pu, Sr and Np Loading

Figure 15 shows the uranium, neptunium, strontium and plutonium data side by side. Looking at the uranium plot in Figure 15, the data at large loadings (indicated by the symbol "+" in both figures) correlate with the large Pu loading (shown with the symbol "+") shown in the Pu figure. This may be evidence of co-precipitation or specific adsorption on deposited uranium. We eliminated the Pu data at this loading since the final Pu concentration fell below the detection limit. At the same time neptunium also largely loaded on MST while strontium did not load to the same extent. The large uranium sorption appears to enhance both plutonium and neptunium loading and inhibits strontium loading.

Conclusions

We identified three models, out of 29 examined, that can fit and predict uranium, strontium and plutonium loading on MST. Two of the models – the Fowler-Guggenheim-Jovanovic-Freundlich and Fowler-Guggenheim-Langmuir-Freundlich (FG-JF and FG-LF) – are inverse model. The Dubinin-Astashov model is a conventional isotherm. We recommend the DA model for its minimal amount of parameters and for ease of application. The DA model successfully reproduced the uranium, strontium and

plutonium data set. The binding energies derived from the model explain the observed irreversibility of the adsorption process on MST.

To enhance our predictive tools, we recommend additional testing that includes wider range of actinide and strontium concentrations, verifying in particular the limited data set for high plutonium concentrations. We also recommend adding Am and Cm to future experimental studies to expand our data set on these two actinides.

We recommend a more complete analysis of the implications that increased uranium trapping in the micropores has on facility operation and risk of nuclear criticality.

We recommend continuing the modeling analysis for non-equilibrium data at shorter processing times. Analyzing this data offers the greatest benefits for assessing options to accelerate production rate for the facilities.

We also recommend additional testing of single component and binary actinide solutions. These studies will either verify the parameters found from the multi-component study or indicate the need to explicitly develop the forms of the model that show binary interaction

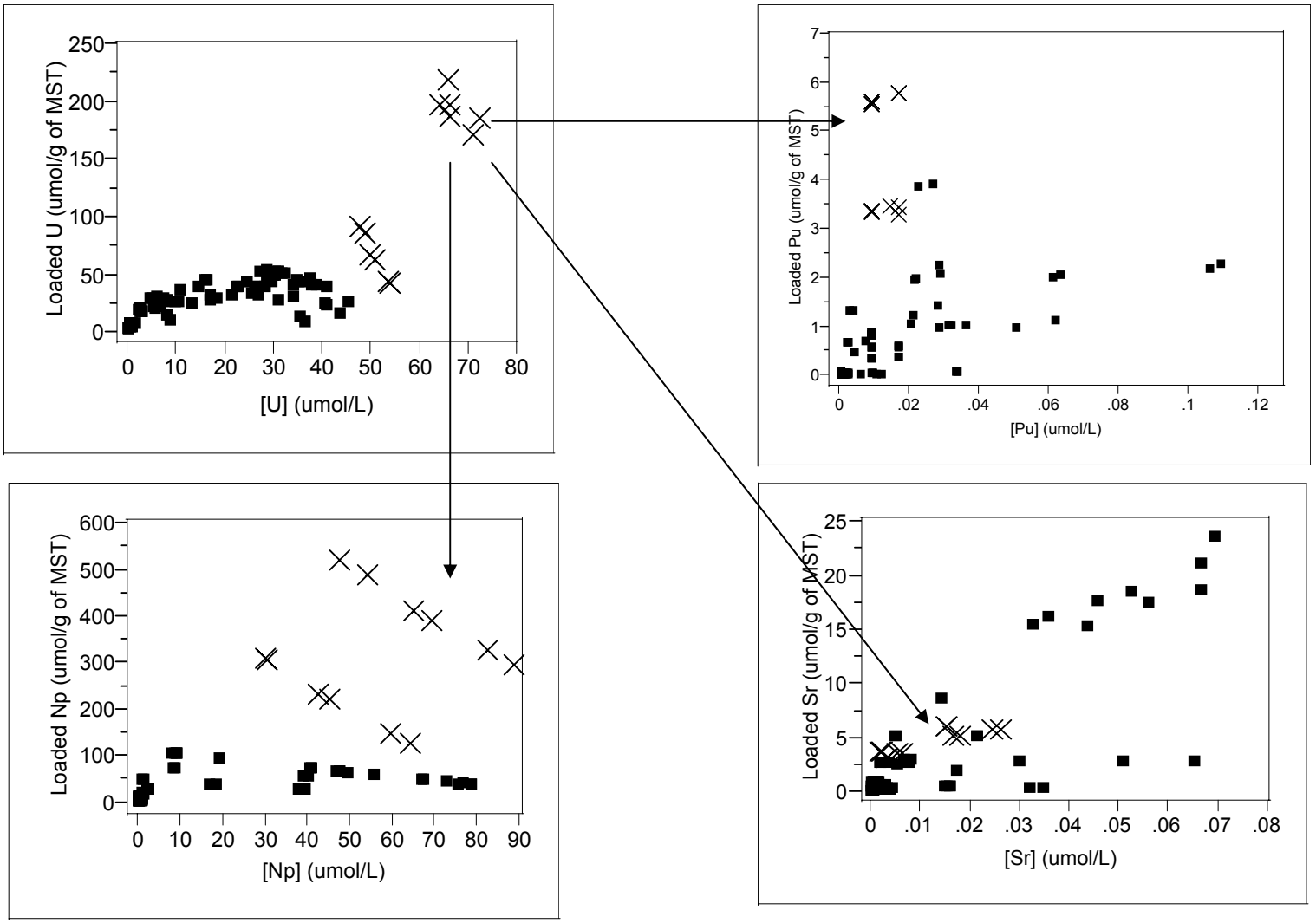

Figure 15. The effect of excess uranium loading on the Np, Sr and Pu loading.

Appendix A. Isotherm Models Evaluated during this study

The following list shows the mathematical form of the isotherms evaluated during this study. For purposes of brevity, we omit the full definition of the mathematical terms and refer the interested reader to the references for the model.

1. Langmuir Isotherm[39]

$$Y = \frac{Y_m K X}{1 + K X}$$

2. Competitive Quadratic[38]

$$Y/Y_m = \frac{a_i X_i + a_{ij} X_i X_j}{1 + b_i X_i + b_j X_j + b_{ij} X_i X_j}$$

3. Freundlich Isotherm[39]

$$Y = K X^n$$

4. Sips (Langmuir-Freundlich)[40]

$$Y = Y_m \frac{b X^n}{1 + b X^n}$$

5. Dubinin-Astashov (thermodynamically consistent)[41]

$$Y = Y_m \exp\left[- a \left(\frac{RT}{E} \right)^n \left(Ln \left(\frac{S}{X} \right) \right)^n \right]$$

6. Myers[39]

$$X = \frac{Y}{H} \exp\left(K Y^n \right)$$

7. Redlich-Peterson[39]

$$Y = \frac{K_1 X}{1 + K_2 X^n}$$

8. Radke-Prausnitz[39]

$$1/Y = \frac{1}{aX} + \frac{1}{bX^n}$$

9. Toth[17]

$$Y = \frac{Y_m X}{\left(b + X^n\right)^{1/n}}$$

10. Volmer [39]

$$bX = \left(\frac{\theta}{1-\vartheta}\right)\exp\left(\frac{\theta}{1-\vartheta}\right);\ \theta = Y/Y_m$$

11. Temkin (thermodynamically consistent)[10]

$$Y = \frac{RT}{b} Ln(aX)$$

12. Gu (Multilayer formation-Langmuir)[42]

$$Y = Y_m \frac{a\,X/X_o\left(n^{-1} + b\left(X/X_o\right)^{n-1}\right)}{1 + a\,X/X_o\left(1 + b\left(X/X_o\right)^{n-1}\right)}$$

13. Frumkin-Damaskin[15]

$$bX = \frac{\theta}{n(1-\theta)^n}\exp(-2a\theta);\ \theta = \frac{Y}{Y_m}$$

14. Ideal Absorbed Solution Theory (Freundlich Derived) (thermodynamically consistent) [40]

$$X = \frac{\theta_i}{\sum_1^N \theta_j}\left[\frac{\sum_1^N n_j\theta_j}{n_i K_i}\right]^{n_i};\theta = Y/Y_m$$

15. Le Van-Vermeulen Competitive (Up to second order) (thermodynamically consistent)[18]

$$Y_i \Big/ Y_{m_i} = \left(\frac{a_i X_i + a_j X_j}{b_i X_i + b_j X_j} b_i X_i \Big/ 1 + b_i X_i + b_j X_j \right) + \left(\frac{a_i}{b_i} - \frac{a_j}{b_j} \right) \frac{b_i b_j X_i X_j}{(b_i X_i + b_j X_j)^2} Ln(1 + b_i X_i + b_j X_j)$$

16. Jovanovic[43]

$$Y \Big/ Y_m = a\left(1 - e^{-bX}\right)$$

17. Sheindorf-Rebuhn-Sheintuch [30]

$$\frac{Y_i}{Y_{m_i}} = a_i X_i \left(\sum_1^N a_{ij} X_j \right)^{n_i - 1}$$

18. Vacancy Solution Theory (thermodynamically consistent)[19]

$$X = \left(\frac{\theta}{b(1 - \vartheta)} \right) \left[\frac{b_{12}\left(1 - (1 - b_{21})\theta\right)}{b_{12} + (1 - b_{12})\theta} \right] \exp\left[- \frac{b_{21}(1 - b_{21})\theta}{1 - (1 - b_{21})\theta} - \frac{(1 - b_{12})\theta}{b_{12} + (1 - b_{12})\theta} \right]; \theta = Y \Big/ Y_m$$

19. Myers-Valenzuela[44]

$$Y \Big/ Y_m = \frac{1}{2b} Ln \frac{a + X \exp(b)}{a + X \exp(-b)}$$

20. Khan[45]

$$Y \Big/ Y_m = \frac{aX}{(1 + aX)^b}$$

21. Khan-Riazi-AlRoomi[46]

$$X = Y \exp\left[(1 - Y)^2 \left(a + bY + cY^n \right) \right]$$

22. Jaroniec-Marczewski[47]

$$Y/Y_m = \frac{(KX)^a}{\left[1+(KX)^b\right]^{a/b}}$$

23. Fowler-Guggenheim[48]

$$bX = \frac{\theta}{1-\theta}\exp(-2a\theta)$$

24. Fowler-Guggenheim-Jovanovich-Freundlich [25]

$$Y/Y_m = \left[1 - e^{\left(-\left(aX\,e^{bY/Y_m}\right)^c\right)}\right]$$

25. Fowler-Guggenheim-Langmuir-Freundlich [25]

$$\theta = \frac{\left(aX\,e^{b\theta}\right)^c}{1+\left(aX\,e^{b\theta}\right)^c};\ \theta = Y/Y_m$$

26. Virial[39]

$$\frac{bX}{Y} = \exp\left(2a_1Y + \frac{3}{2}a_2Y^2 + \ldots + \frac{n+1}{n}a_nY^n\right)$$

27. B.E.T.-Multilayer (Brunauer-Emmett-Teller)[39]

$$Y/Y_m = \frac{cX}{\left(1-\frac{X}{S}\right)\left(1+cX-\frac{X}{S}\right)}$$

28. Sigmoidal[39]

$$Y = \frac{(a-b)}{\left[1+e^{\frac{(X-c)}{d}}\right]} + b$$

29. Generalized Isotherm [39]

$$\frac{bX}{Y} = 1 + a_1Y + a_2Y^2 + \ldots + a_nY^n$$

Appendix B. Experimental Data used in Modeling Effort.

The following tables contain the experimental data used in this modeling study. The values shown include many more digits than experimentally significant. The authors used the extraneous digits to avoid numerical round-off errors during calculations.

Table B1. The plutonium experimental data set.

Data Number	Data Not Selected	Reason	[Pu] (umole/L)	Loaded Pu (umole/g of MST)	[Pu] initial (umole/L)	MST g/L
1	X	Detection Limit	0.008995816	0.842	0.027866	1.1
2	X	Detection Limit	0.008995816	0.841	0.004761	2
3	X	Detection Limit	0.008995816	0.807170027	0.007264	0.2
4	X	Detection Limit	0.008995816	0.807170027	0.003138	1.1
5	X	Detection Limit	0.008995816	0.803081019	0.003137	1.1
6	X	Detection Limit	0.008995816	0.803081019	0.003138	1.1
7	X	Detection Limit	0.008995816	0.841517687	0.004761	2
8	X	Detection Limit	0.008995816	0.841517687	0.003137	1.1
9	X	Detection Limit	0.008995816	0.807170027	0.003137	1.1
10	X	Detection Limit	0.008995816	0.807170027	0.001961	2
11	X	Detection Limit	0.008995816	0.803081019	0.003137	1.1
12	X	Detection Limit	0.008995816	0.803081019	0.002344	0.2
13	X	Detection Limit	0.008995816	0.841517687	0.007264	2
14	X	Detection Limit	0.008995816	0.841517687	0.004688	0.2
15	X	Detection Limit	0.008995816	0.807170027	0.002344	2
16	X	Detection Limit	0.008995816	0.807170027	0.004688	0.2
17			0.008995816	0.803081019	0.003137	1.1
18			0.008995816	0.803081019	0.002344	2
19			0.001469418	0.023997308	0.003137	1.1
20			0.000163735	0.025184292	0.001961	2
21			0.00047153	0.002424132	0.007264	2
22			0.000338078	0.002545452	0.003138	1.1
23			0.000531154	0.002368612	0.002344	0.2
24			0.000364424	0.002520185	0.003138	1.1
25			0.001217517	0.024226308	0.007264	0.2
26			0.002382556	0.023167182	0.027866	1.1
27			0.000948991	0.001990076	0.027866	1.1
28			0.000996441	0.00194694	0.003138	1.1
29			0.000502572	0.002394596	0.001961	0.2
30			0.00085985	0.002069798	0.003138	1.1
31			0.002571481	0.022995432	0.26573	0.4
32			0.002550489	0.023014515	0.001961	0.2
33			0.001642942	0.001359213	0.012018	2
34			0.001476868	0.001510188	0.027866	1.1
35			0.000609755	0.002297156	0.26573	0.4
36			0.000793158	0.002130427	0.027866	1.1
37			0.000676982	0.020057252	0.027866	1.1
38			0.000738907	0.019747625	0.26573	0.2
39			0.000265421	0.034991735	0.26573	0.2

Table B1. The plutonium experimental data set.

Data Number	Data Not Selected	Reason	[Pu] (umole/L)	Loaded Pu (umole/g of MST)	[Pu] initial (umole/L)	MST g/L
40			0.001002372	0.031306979	0.17886	0.4
41			0.000635955	0.008541303	0.041139	2
42			0.000981325	0.006814458	0.012018	2
43	X	Detection Limit	0.014298434	3.436876029	0.27497	0.4
44	X	Detection Limit	0.014298434	3.436876029	0.041139	2
45	X	Detection Limit	0.008995816	3.328451883	0.93467	1.1
46	X	Detection Limit	0.008995816	3.328451883	0.93377	1.1
47	X	Detection Limit	0.008995816	3.310460251	0.89688	1.1
48	X	Excessive Loading	0.016947475	3.270701958	0.89688	1.1
49			0.000193123	0.002283973	0.89238	1.1
50			0.000488057	0.002136507	0.89238	1.1
51			0.000910439	0.003176665	0.93467	1.1
52			0.000661328	0.00330122	0.93467	1.1
53			0.00071932	0.000812448	0.89688	1.1
54			0.000802685	0.000770765	0.89688	1.1
55	X	Detection Limit	0.014298434	0.343687603	0.89238	1.1
56	X	Detection Limit	0.014298434	0.343687603	0.89238	1.1
57	X	Detection Limit	0.008995816	0.332845188	0.93467	1.1
58	X	Detection Limit	0.008995816	0.332845188	0.93467	1.1
59	X	Detection Limit	0.008995816	0.331046025	0.89688	1.1
60	X	Detection Limit	0.008995816	0.331046025	0.89688	1.1
61			0.037365191	0.01887075	0.89238	1.1
62			0.031172646	0.049833479	0.89238	1.1
63			0.01055753	0.007303521	0.67469	0.2
64			0.011921706	0.000482644	0.67469	0.2
65			0.001562497	0.001993601	0.67109	0.2
66	X	Detection Limit	0.002238944	-0.001388634	0.67469	2
67	X	Detection Limit	0.014298434	5.775788163	0.67469	2
68	X	Detection Limit	0.014298434	5.775788163	0.67109	2
69	X	Detection Limit	0.008995816	5.577405858	0.67109	2
70	X	Detection Limit	0.008995816	5.577405858	1.1245	0.2
71	X	Detection Limit	0.008995816	5.532426778	1.1245	0.2
72	X	Detection Limit	0.008995816	5.532426778	1.1155	0.2
73			0.00855411	0.016292616	1.1155	0.2
74			0.005510316	0.017814513	1.1245	2
75			0.006138789	0.002939723	1.1245	2
76			0.002322064	0.004848085	1.1155	2
77			0.000881287	0.000539965	0.012018	0.2
78			0.000604991	0.000678113	0.012018	0.2
79	X	Detection Limit	0.014298434	0.577578816	0.70167	0.2
80	X	Detection Limit	0.014298434	0.577578816	0.70167	0.2
81	X	Detection Limit	0.008995816	0.557740586	0.70167	2
82	X	Detection Limit	0.008995816	0.557740586	0.70167	2
83	X	Detection Limit	0.008995816	0.553242678	1.1695	0.2
84			0.016947475	0.549266848	1.1695	0.2
85			0.002531547	0.657985597	1.1695	2

Table B1. The plutonium experimental data set.

Data Number	Data Not Selected	Reason	[Pu] (umole/L)	Loaded Pu (umole/g of MST)	[Pu] initial (umole/L)	MST g/L
86			0.002024928	0.659252144	1.1695	2
87			0.002772382	1.314767021	0.67109	0.2
88			0.003836605	1.309445902	1.1155	2
89			0.026642499	3.897867073	0.43301	0.4
90			0.022264373	3.83967003	0.50562	0.4
91			0.021516888	1.921703728	0.7902	0.4
92			0.021944023	1.947331783	0.80088	0.4
93			0.028404428	2.22	0.7902	0.2
94			0.028884954	2.06	0.80622	0.2
95			0.028297645	0.949	0.58731	0.4
96			0.036039453	0.992	0.40805	0.4
97			0.020502444	1.03	0.91834	0.4
98			0.031287584	1	0.85427	0.4
99			0.031981678	1	0.041139	0.2
100			0.031234193	1	0.43301	0.4
101			0.106249647	2.150354036	0.43301	0.4
102			0.050722193	0.941030165	0.43301	0.4
103			0.004132524	0.436824868	0.43301	0.4
104			0.028137469	1.397930342	0.041139	0.2
105			0.020929579	1.211726501	0.42713	0.4
106			0.061934468	1.093196744	0.84893	0.4
107			0.108919236	2.263811573	0.49921	0.4
108			0.007314674	0.669132513	0.87029	0.4
109			0.063002303	2.018209374	0.96639	0.4
110			0.060866632	1.97015677	1.0144	0.4

Table B2. The strontium experimental data set.

Data Number	Data not Selected	Reason	[Sr] (umole/L)	Loaded Sr (umole/g of MST)	Initial[Sr] (umol/L)	MST g/L
1	X	Detection Level	0	0.068685024	0.075554	1.1
2	X	Detection Level	0	0.028418169	0.056836	2
3			5.66769E-06	0.028415336	0.056836	2
4			1.71186E-05	0.028295481	0.056608	2
5	X	Detection Level	3.59134E-05	0.362912881	0.72586	2
6	X	Detection Level	3.59462E-05	0.362912865	0.72586	2
7			3.81211E-05	0.832070924	0.91532	1.1
8	X	Detection Level	3.82094E-05	0.344651062	0.68934	2
9	X	Detection Level	3.82201E-05	0.344651057	0.68934	2
10			8.25253E-05	0.028262778	0.056608	2
11			0.000169142	0.028333599	0.056836	2
12			0.000195815	0.87965432	0.96782	1.1
13			0.000337576	0.748795642	0.82401	1.1
14			0.000353292	0.06836385	0.075554	1.1
15			0.000359763	0.309110235	0.61858	2
16			0.000397847	0.748740851	0.82401	1.1
17			0.000411364	0.028212487	0.05683	2
18			0.00044985	0.879423379	0.96782	1.1
19			0.000459491	0.879414615	0.96782	1.1
20			0.05245	18.389	7.4082	0.4
21			0.000463902	0.068263295	0.07555	1.1
22			0.000472247	0.831676264	0.91532	1.1
23			0.000473062	0.068254967	0.07555	1.1
24			0.000526875	0.068206047	0.07555	1.1
25			0.000533973	0.30902313	0.61858	2
26			0.000545966	0.57151428	1.1436	2
27			0.000581783	0.748573636	0.82401	1.1
28			0.00066223	0.514391551	1.0294	2
29			0.00066687	0.879226088	0.96782	1.1
30			0.000672172	0.068073958	0.07555	1.1
31			0.000679451	0.748484847	0.82401	1.1
32			0.000712814	0.748454517	0.82401	1.1
33			0.000721968	0.068028689	0.07555	1.1
34			0.0007743	0.831401671	0.91532	1.1
35			0.000812862	0.514316235	1.0294	2
36			0.000861743	0.831322177	0.91532	1.1
37			0.001088854	0.831115713	0.91532	1.1
38			0.001107642	0.067678077	0.07555	1.1
39			0.001123275	0.571225626	1.1436	2
40			0.001165064	0.067625875	0.07555	1.1
41			0.00118555	0.878754561	0.96782	1.1
42			0.001195969	0.748015285	0.82401	1.1
43			0.00124874	0.067549806	0.07555	1.1
44			0.001307793	0.067496122	0.07555	1.1
45			0.001393183	0.067418494	0.07555	1.1

Table B2. The strontium experimental data set.

Data Number	Data not Selected	Reason	[Sr] (umole/L)	Loaded Sr (umole/g of MST)	Initial[Sr] (umol/L)	MST g/L
46			0.001421664	0.046538654	0.09449	2
47			0.001437425	0.046530774	0.09449	2
48			0.001509213	0.604130123	1.2098	2
49			0.001515032	0.067307722	0.07555	1.1
50			0.001554775	0.046472099	0.09449	2
51			0.001621171	0.067211232	0.07555	1.1
52			0.001630079	0.83062369	0.91532	1.1
53			0.00164585	0.067188797	0.07555	1.1
54			0.001834913	0.067016922	0.07555	1.1
55			0.001926647	0.603921406	1.2098	2
56	X	Detection Level	0.001996634	2.562915285	1.0272	0.4
57	X	Detection Level	0.001996674	2.562915185	1.0272	0.4
58			0.002001014	0.273035334	0.0566	0.2
59			0.002017459	0.046240757	0.09449	2
60			0.002061161	0.066811242	0.07555	1.1
61			0.002094289	0.272568956	0.0566	0.2
62			0.002102266	3.618797046	0.72586	0.2
63			0.002149888	0.87787789	0.96782	1.1
64			0.00272376	0.066208879	0.07555	1.1
65			0.002745016	0.270456615	0.05683	0.2
66			0.002938317	0.26949011	0.05683	0.2
67			0.003085801	3.077472158	0.61858	0.2
68			0.003257952	3.076611404	0.61858	0.2
69			0.003288297	0.267740209	0.05683	0.2
70			0.003456155	3.612027601	0.72586	0.2
71			0.003492353	2.653332572	1.0648	0.4
72			0.003873667	0.045312653	0.09449	2
73			0.004030469	0.045234252	0.09449	2
74			0.004075412	0.263804633	0.05683	0.2
75	X	Detection Level	0.004851177	5.111557855	1.0272	0.2
76	X	Detection Level	0.004870597	5.111460756	1.0272	0.2
77			0.005268574	3.420358799	0.68934	0.2
78			0.005304662	2.503312378	1.0066	0.4
79			0.006294791	3.415227711	0.68934	0.2
80			0.006750559	2.827152038	1.1376	0.4
81			0.00727424	2.573544159	1.0367	0.4
82			0.007499421	2.571723291	1.0362	0.4
83			0.008070472	2.823852257	1.1376	0.4
84			0.01330216	5.982336496	1.2098	0.2
85			0.014025605	8.584840817	3.448	0.4
86			0.014772494	5.974984826	1.2098	0.2
87			0.014823621	0.398376761	0.09449	0.2
88			0.01578704	0.393559662	0.09449	0.2
89			0.015964378	0.392672974	0.09449	0.2
90			0.016375423	5.065349548	1.0294	0.2

Table B2. The strontium experimental data set.

Data Number	Data not Selected	Reason	[Sr] (umole/L)	Loaded Sr (umole/g of MST)	Initial[Sr] (umol/L)	MST g/L
91			0.016408441	0.390452657	0.09449	0.2
92			0.017075723	1.796738261	0.73577	0.4
93			0.017871227	5.057870524	1.0294	0.2
94	X	Detection Level	0.021154544	4.994005883	1.02	0.2
95	X	Detection Level	0.021167932	5.118677388	1.0449	0.2
96			0.024342116	5.596162051	1.1436	0.2
97			0.026123578	5.587254743	1.1436	0.2
98			0.029914906	2.769241173	1.1376	0.4
99			0.032012677	0.312431478	0.09449	0.2
100			0.032521254	15.35292157	6.1737	0.4
101			0.03477421	0.298623812	0.09449	0.2
102			0.035788856	16.1275457	6.4868	0.4
103			0.043941696	15.22218962	6.1328	0.4
104			0.045726185	17.59592527	7.0841	0.4
105	X	Exceeds total mass equivalents for available sites	0.050927845	2.716708825	1.1376	0.4
106			0.056004145	17.46554615	7.0422	0.4
107	X	Exceeds total mass equivalents for available sites	0.065106723	2.68126163	1.1376	0.4
108			0.066589985	21.00238487	8.4675	0.4
109	X	Exceeds total mass equivalents for available sites	0.066649828	18.56293621	7.4918	0.4
110			0.068988778	23.43843079	9.4444	0.4

Table B3. The neptunium experimental data set.

Data Number	Data Not Used	Reason	[Np] (umole/L)	Np (umole/g of MST)	[Np] initial (μMol/L)	MST g/L
1	X	Detection Limit	0.008438819	4.127349444	4.548523	1.1
2	X	Detection Limit	0.008438819	4.127349444	4.548523	1.1
3	X	Detection Limit	0.008438819	4.127349444	4.548523	1.1
4	X	Detection Limit	0.008438819	4.127349444	4.548523	1.1
5	X	Detection Limit	0.008438819	0.713080169	1.434599	2
6	X	Detection Limit	0.008438819	0.713080169	1.434599	2
7	X	Detection Limit	0.015021097	1.796854622	1.991561	1.1
8	X	Detection Limit	0.015021097	1.796854622	1.991561	1.1
9	X	Detection Limit	0.015021097	1.796854622	1.991561	1.1
10	X	Detection Limit	0.015021097	1.796854622	1.991561	1.1
11	X	Detection Limit	0.015021097	1.796854622	1.991561	1.1
12	X	Detection Limit	0.015021097	1.796854622	1.991561	1.1
13	X	Detection Limit	0.015021097	7.393248945	1.493671	0.2
14	X	Detection Limit	0.015021097	7.393248945	1.493671	0.2
15	X	Detection Limit	0.015021097	0.739324895	1.493671	2
16	X	Detection Limit	0.015021097	0.739324895	1.493671	2
17	X	Detection Limit	0.015021097	1.23721519	2.489451	2
18	X	Detection Limit	0.015021097	1.23721519	2.489451	2
19	X	Detection Limit	0.017890295	2.983352512	3.299578	1.1
20	X	Detection Limit	0.017890295	2.983352512	3.299578	1.1
21	X	Detection Limit	0.017890295	2.983352512	3.299578	1.1
22	X	Detection Limit	0.017890295	2.983352512	3.299578	1.1
23	X	Detection Limit	0.017890295	2.983352512	3.299578	1.1
24	X	Detection Limit	0.017890295	2.983352512	3.299578	1.1
25			0.017890295	12.31561181	2.481013	0.2
26	X	Detection Limit	0.017890295	1.231561181	2.481013	2
27	X	Detection Limit	0.017890295	1.231561181	2.481013	2
28			0.103957215	2.291081937	1.02039	0.4
29			0.104472574	6.650632911	1.434599	0.2
30			0.108607595	4.03628692	4.548523	1.1
31			0.108860759	6.628691983	1.434599	0.2
32			0.109496181	1.990257431	0.905599	0.4
33			0.110740928	11.85135865	2.481013	0.2
34			0.128185654	4.018488684	4.548523	1.1
35			0.141007374	3.935148079	1.715067	0.4
36			0.147031994	3.92008653	1.715067	0.4

Table B3. The neptunium experimental data set.

Data Number	Data Not Used	Reason	[Np] (umole/L)	Np (umole/g of MST)	[Np] initial (μMol/L)	MST g/L
37			0.165127426	1.980727426	4.126582	2
38			0.202700422	6.296413502	2.721266	0.4
39			0.204664979	1.96095865	4.126582	2
40			0.216421293	3.88359624	1.76986	0.4
41			0.225000581	1.441689422	0.801676	0.4
42			0.240590717	4.257805907	1.943713	0.4
43			0.244882905	2.009609976	1.048727	0.4
44			0.254626743	3.693276711	1.731937	0.4
45			0.279845062	7.176107718	1.715067	0.2
46			0.296503541	1.888175628	1.051774	0.4
47			0.31907173	4.321729958	2.047764	0.4
48			0.346944344	6.84061131	1.715067	0.2
49			0.351123699	1.443499031	0.928523	0.4
50			0.378575485	1.631083091	1.031009	0.4
51			0.425170725	1.239069574	0.920799	0.4
52			0.479436458	6.111413781	1.701719	0.2
53			0.48556962	3.905485232	2.047764	0.4
54			0.503106377	1.282707115	1.016189	0.4
55			0.503610366	6.07880536	1.719371	0.2
56			0.504050633	3.326033755	7.156118	2
57			0.553670886	3.301223629	7.156118	2
58			0.628523207	3.548101266	2.047764	0.4
59			0.629873418	3.544725738	2.047764	0.4
60			0.667237131	9.11107173	2.489451	0.2
61			0.728438819	3.298312236	2.047764	0.4
62			0.771633755	8.589088608	2.489451	0.2
63			0.824921519	16.5083038	4.126582	0.2
64			0.872132547	3.211493527	2.15673	0.4
65			0.908606386	0.968275351	1.295917	0.4
66			0.986160338	45.07654008	91.13924	2
67			1.167520675	14.79530802	4.126582	0.2
68			1.220253165	44.95949367	91.13924	2
69			2.429451477	23.71772152	7.172996	0.2
70			2.496202532	23.38396624	7.172996	0.2
71			7.953080169	102.4745685	120.6751	1.1
72			8.107257384	71.47379747	151.0549	2
73			8.57628692	71.2392827	151.0549	2
74			8.606919831	101.8801688	120.6751	1.1
75			8.832151899	101.6754124	120.6751	1.1
76			8.987088608	101.5345608	120.6751	1.1
77			9.061265823	101.467127	120.6751	1.1
78			16.55974684	36.02392405	88.60759	2
79			18.43265823	35.08746835	88.60759	2
80			19.05400844	92.3828155	120.6751	1.1
81			29.91873418	306.1025316	91.13924	0.2
82			30.26312236	304.3805907	91.13924	0.2

Table B3. The neptunium experimental data set.

Data Number	Data Not Used	Reason	[Np] (umole/L)	Np (umole/g of MST)	[Np] initial (μMol/L)	MST g/L
83			39.04278481	53.89632911	146.8354	2
84			40.05383966	53.39080169	146.8354	2
85			40.38295359	69.92420407	117.2996	1.1
86			40.95679325	69.40253165	117.2996	1.1
87			42.63848101	229.8455696	88.60759	0.2
88			43.5657384	22.52092827	88.60759	2
89			43.83392405	22.38683544	88.60759	2
90			45.0307173	217.8843882	88.60759	0.2
91			46.70751055	64.17460683	117.2996	1.1
92			47.39206751	518.3139241	151.0549	0.2
93	X	Detection Limit	47.57637131	63.38473341	117.2996	1.1
94	X	Detection Limit	47.57637131	63.38473341	117.2996	1.1
95			49.52185654	61.61611047	117.2996	1.1
96			53.87459916	485.9012658	151.0549	0.2
97			61.48345992	51.66252397	118.3122	1.1
98			64.00514768	123.0122363	88.60759	0.2
99			64.98860759	409.2341772	146.8354	0.2
100			66.03848101	112.8455696	88.60759	0.2
101			69.28953586	387.7295359	146.8354	0.2
102			73.54852321	40.69428462	118.3122	1.1
103			76.56413502	37.95281933	118.3122	1.1
104			77.15156118	37.41879555	118.3122	1.1
105			78.03063291	36.61963943	118.3122	1.1
106			78.40219409	36.28185654	118.3122	1.1
107			88.99265823	29.34333333	147.6793	2
108			92.31535865	27.68198312	147.6793	2
109			95.91409283	258.8261603	147.6793	0.2
110			97.12008439	252.7962025	147.6793	0.2

Table B4. The uranium experimental data.

Data Number	Data not used	Reason	[U] (umole/L)	Loaded U (umole/g of MST)	[U] initial (μMol/L)	MST g/L
1	x	Detection Limit	0.008403361	3.180672269	6.3697	2
2	x	Detection Limit	0.008403361	3.180672269	6.3697	2
3	x	Detection Limit	0.008403361	3.281512605	6.5714	2
4	x	Detection Limit	0.008403361	2.903361345	5.8151	2
5	x	Detection Limit	0.008403361	2.903361345	5.8151	2
6			0.047394958	3.262016807	6.5714	2
7			0.314369748	6.742475172	7.7311	1.1
8			0.345882353	7.47776929	8.5714	1.1
9			0.351176471	7.625744843	8.7395	1.1
10			0.377394958	6.685179526	7.7311	1.1
11			0.383445378	5.270462185	10.924	2
12			0.407815126	4.62802521	9.6639	2
13			0.411512605	7.570893812	8.7395	1.1
14			0.413445378	5.255462185	10.924	2
15			0.41697479	7.413139801	8.5714	1.1
16			0.424453782	7.559129106	8.7395	1.1
17			0.429579832	6.637738732	7.7311	1.1
18			0.432184874	7.55210084	8.7395	1.1
19			0.438487395	7.393582888	8.5714	1.1
20			0.448991597	7.536822002	8.7395	1.1
21			0.449831933	7.383269672	8.5714	1.1
22			0.455966387	7.377692895	8.5714	1.1
23			0.485630252	6.586783804	7.7311	1.1
24			0.508739496	4.577563025	9.6639	2
25			0.511848739	6.562948816	7.7311	1.1
26			0.54487395	6.532925898	7.7311	1.1
27			0.617310924	7.231016043	8.5714	1.1
28			0.673697479	4.650546218	9.9748	2
29			0.713865546	4.630462185	9.9748	2
30			1.305294118	6.758365164	8.7395	1.1
31			2.199915966	18.07605042	5.8151	0.2
32			2.334285714	17.40420168	5.8151	0.2
33			2.508487395	20.31470588	6.5714	0.2
34			2.550840336	20.10294118	6.5714	0.2
35			2.815546218	17.7710084	6.3697	0.2
36			2.900756303	17.4289916	6.3866	0.2
37			4.675714286	29.1747479	63.025	2
38			4.994705882	29.0152521	63.025	2
39			5.334789916	21.64537815	9.6639	0.2
40			5.72907563	19.67394958	9.6639	0.2
41			5.92512605	29.89457983	65.714	2
42			6.344201681	22.90084034	10.924	0.2
43			6.681512605	21.21428571	10.924	0.2

Table B4. The uranium experimental data.

Data Number	Data not used	Reason	[U] (umole/L)	Loaded U (umole/g of MST)	[U] initial (μMol/L)	MST g/L
44			7.273445378	29.22042017	65.714	2
45			7.973265412	25.39963534	18.133	0.4
46			8.011008403	13.72647059	10.756	0.2
47			8.029134864	27.08234349	18.862	0.4
48			8.681596639	10.37352941	10.756	0.2
49			9.606470588	26.24718487	62.101	2
50			10.27344538	25.91369748	62.101	2
51			10.87142555	35.44980916	25.051	0.4
52			13.22752749	24.57049501	23.056	0.4
53			14.38852611	38.7760839	29.899	0.4
54			15.82579832	44.60810924	105.04	2
55			16.28697479	44.37752101	105.04	2
56			16.72306411	27.74539406	27.821	0.4
57			16.82296227	31.26855767	29.33	0.4
58			18.33731948	28.25576597	29.64	0.4
59			21.47247615	31.24467433	33.97	0.4
60			22.46702699	38.55148238	37.888	0.4
61			22.5677754	38.29961138	37.888	0.4
62			24.27344538	42.48512605	109.24	2
63			24.43386555	42.40491597	109.24	2
64			25.43830881	33.28239753	38.751	0.4
65			25.95134454	38.705	103.36	2
66			26.02613445	38.66760504	103.36	2
67			26.74391033	31.75087484	39.444	0.4
68			27.1905042	51.52276547	83.866	1.1
69			28.06013552	39.12693543	43.711	0.4
70			28.59697951	46.45320218	37.888	0.2
71			28.65672269	53.12647059	49.907	0.4
72			29.39823615	42.44691897	37.888	0.2
73			29.88537815	49.07288006	83.866	1.1
74			30.02394958	48.94690604	83.866	1.1
75			30.16663866	52.02574484	87.395	1.1
76			30.20983193	48.77792208	83.866	1.1
77			30.36252101	48.63911383	83.866	1.1
78			30.73394958	51.51000764	87.395	1.1
79			30.90243697	27.44306723	41.88	0.4
80			30.9305042	51.33132162	87.395	1.1
81			31.72218487	50.61161192	87.395	1.1
82			32.25941176	50.12322383	87.395	1.1
83			33.93890756	30.68676471	46.214	0.4
84			34.12991597	39.44348739	49.907	0.4
85			34.54705882	44.83498854	83.866	1.1
86			34.90352941	43.51779985	82.773	1.1
87			35.19527487	12.62721136	37.721	0.2
88			35.33529412	43.12528648	82.773	1.1

Table B4. The uranium experimental data.

Data Number	Data not used	Reason	[U] (umole/L)	Loaded U (umole/g of MST)	[U] initial (μMol/L)	MST g/L
89			36.0689916	42.45828877	82.773	1.1
90			36.42220466	7.764736875	37.975	0.2
91			37.33285714	45.51100076	87.395	1.1
92			37.83714286	40.85087853	82.773	1.1
93			38.63890756	40.12200153	82.773	1.1
94			40.36243697	23.86218487	49.907	0.4
95			40.93403361	22.43319328	49.907	0.4
96			40.95008403	38.02093201	82.773	1.1
97			43.55537815	15.87983193	49.907	0.4
98			45.23457244	25.37969285	55.386	0.4
99			47.55016807	90.82058824	65.714	0.2
100			48.78739496	84.63445378	65.714	0.2
101			49.82260504	66.01302521	63.025	0.2
102			50.64806723	61.88571429	63.025	0.2
103			53.60420168	42.48319328	62.101	0.2
104			53.86327731	41.18781513	62.101	0.2
105			64.06831933	196.4651261	103.36	0.2
106			65.68571429	217.789916	109.24	0.2
107			65.97521008	195.3340336	105.04	0.2
108			66.27495798	185.4319328	103.36	0.2
109			71.04436975	169.9882353	105.04	0.2
110			72.23487395	185.0441176	109.24	0.2

Table B5. The total equivalence (maximum number of atoms) adsorbed on MST for that testing. We used a maximum of 3 wt % as a criteria for eliminate some plutonium and strontium data.

Sample #	Total/MST In Percent of total Maximum
1	0.052574
2	0.052573
3	0.052708
4	0.052708
5	0.054632
6	0.054632
7	0.052574
8	0.052574
9	0.052708
10	0.052708
11	0.054632
12	0.054632
13	0.052574
14	0.052574
15	0.052708
16	0.052708
17	0.054632
18	0.054632
19	0.003986
20	0.003986
21	0.003803
22	0.003803
23	0.003199
24	0.003199
25	0.003986
26	0.003986
27	0.003803
28	0.003803
29	0.003199
30	0.003199
31	0.003986
32	0.003986
33	0.003803
34	0.003803
35	0.003199
36	0.003199
37	0.014287
38	0.014321
39	0.015746
40	0.015746
41	0.013229
42	0.013229
43	0.216786
44	0.216786

Table B5. The total equivalence (maximum number of atoms) adsorbed on MST for that testing. We used a maximum of 3 wt % as a criteria for eliminate some plutonium and strontium data.

Sample #	Total/MST In Percent of total Maximum
45	0.218314
46	0.218314
47	0.226339
48	0.226339
49	0.001429
50	0.001429
51	0.001575
52	0.001575
53	0.001323
54	0.001323
55	0.021679
56	0.021679
57	0.021831
58	0.021831
59	0.022634
60	0.022634
61	0.029002
62	0.029002
63	0.026178
64	0.026178
65	0.021985
66	0.021985
67	0.361031
68	0.361031
69	0.36301
70	0.36301
71	0.375807
72	0.41676
73	0.002742
74	0.002742
75	0.002618
76	0.002618
77	0.002198
78	0.002198
79	0.036103
80	0.036103
81	0.036301
82	0.036301
83	0.037581
84	0.037581
85	0.040241
86	0.040241
87	0.080481
88	0.080481

Table B5. The total equivalence (maximum number of atoms) adsorbed on MST for that testing. We used a maximum of 3 wt % as a criteria for eliminate some plutonium and strontium data.

Sample #	Total/MST In Percent of total Maximum
89	0.082329
90	0.082741
91	0.04288
92	0.04219
93	0.050011
94	0.045886
95	0.057936
96	0.052855
97	0.052855
98	0.052855
99	0.052855
100	0.052855
101	0.039015
102	0.042672
103	0.029282
104	0.037639
105	0.02641
106	0.033722
107	0.054667
108	0.025498
109	0.036918
110	0.038747

Appendix C. Results of the Fowler-Guggenheim Models.

This section shows the results for the Fowler-Guggenheim-Jovanovich-Freundlich and Fowler-Guggenheim-Langmuir-Freundlich models. These two models successfully captured the non-classical sorption behavior for uranium onto MST at higher mass loadings. Only these two models and the Dubinin-Astashov model adequately replicated this behavior.

$$7)\ [Pu] = \frac{\left[-Ln\left(1 - Loaded\ Pu \,/\, 3.7\right)\right]^{1/3.3}}{1.3 \times e^{35 \times Loaded\ Pu / 3.7}} \qquad FG/JF$$

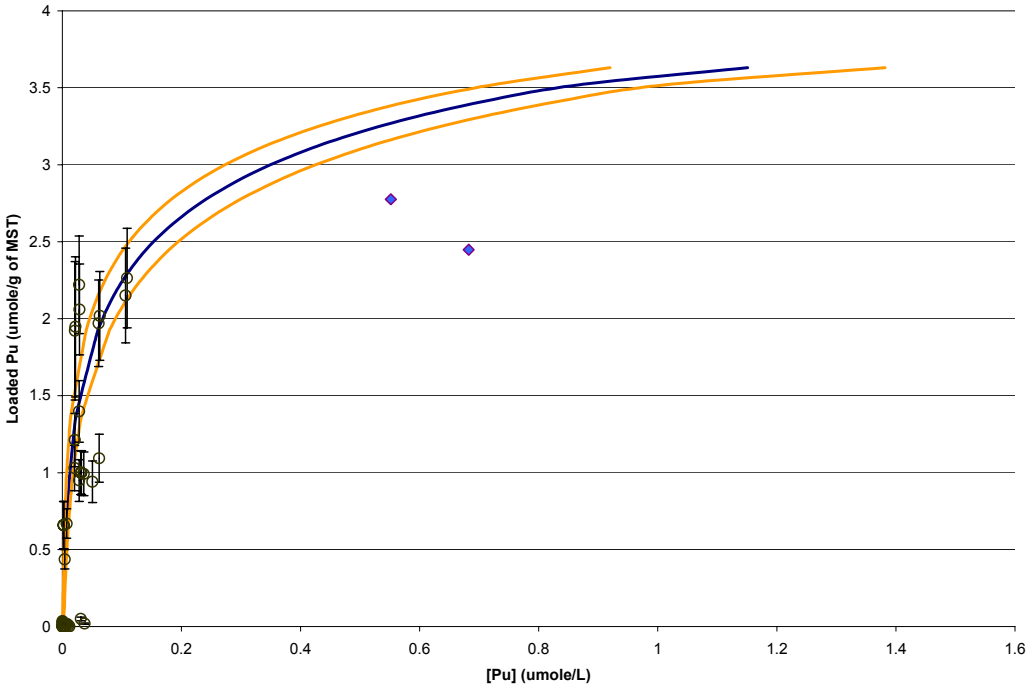

Figure C1. Performance prediction of the FG-JF model for the 168-hour Pu data. The filled points are from radioactive waste testing. The two data points located after [Pu]>0.6 umol/L are actual waste data and we excluded these from the FG-JF model during optimization.

Strontium

The FG-JF models explained 97% of the Sr data. The functional form of the model follows.

$$8)\ [Sr] = \frac{\left[-Ln\left(1-\frac{Loaded\ Sr}{83}\right)\right]^{1/1.31}}{1\times e^{0.1\times\frac{Loaded\ Sr}{83}}} \qquad FG/JF$$

The chosen model indicates the adsorption process takes place on a heterogeneous sorbent. The equation also assumes significant lateral interactions between the adsorbed sorbates. In addition, the successful fitting with the Jovanovic model gives an indication a single monolayer adsorption.

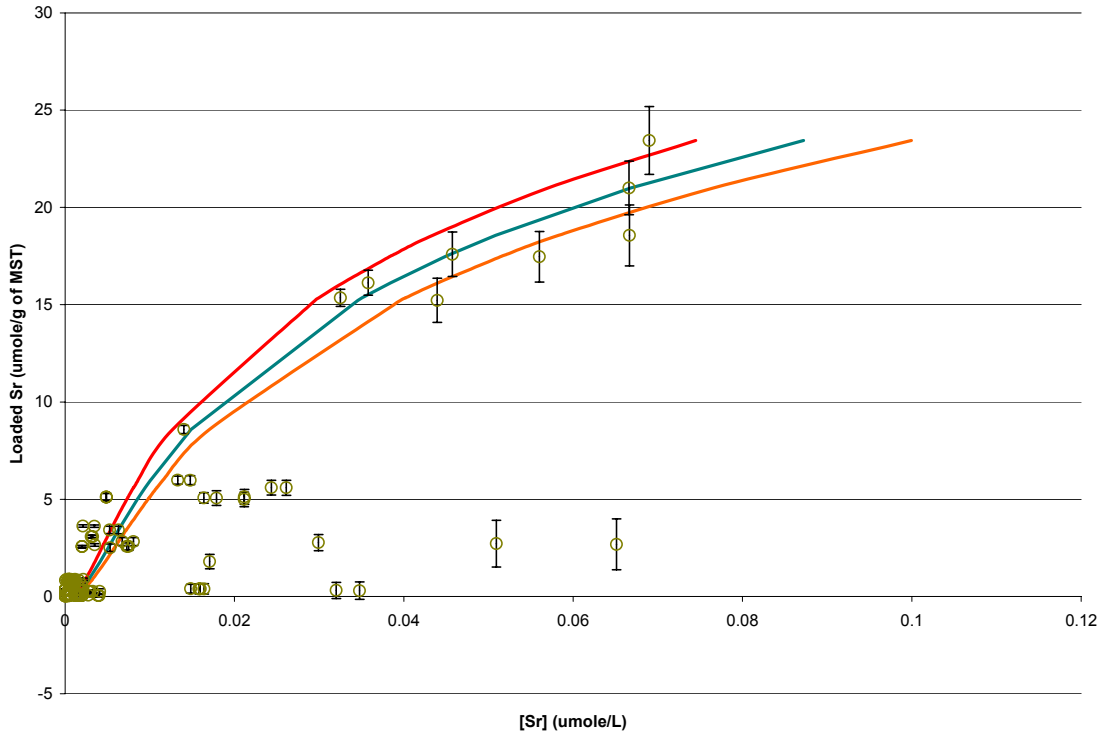

Figure C2. The prediction performance of the FG-JF model on the Sr adsorption data.

Uranium

The uranium concentration range is one order of magnitude larger than the concentration ranges of plutonium and strontium. Evaluation of the uranium data revealed the same functional model found in the previous sorbates. The FG-JF and FG-LF models fitted 97% of the uranium data (see Figure C4). Table C3 shows the fitting performance of these models.

Neptunium

The neptunium concentration range studied here is as large as the uranium data. We tested the fitting performance of each isotherm with the neptunium data. Table C4 shows the fitting results. We omit the figures for neptunium since we still need to assess the complex interaction of uranium and neptunium at high mass loadings. We found significant sensitivity of the neptunium loading isotherm for changes in temperature. We modeled the coefficients of the FG-JF model as a function of temperature. We investigated an exponential function (i.e., Arrhenius function) for fitting each coefficient. The coefficient representing the Fowler-Guggenheim interaction had the highest temperature dependency. We omit the equations at this time due to the uncertainty about the high mass loading data and the most appropriate modeling approach.

Inspection of data in Table C4, the FG-JF model shows low variance and Akaike number and high correlation coefficient. The FG-JF and FG-LF models fitted about 82% of the Np data. Again, the Np data can only be fitted with isotherms that include lateral interactions, heterogeneous sorbents and single layer formation. We did not need to include competitive adsorption by other sorbates.

Tables C1 through C4 summarize the performance of each thermodynamically consistent isotherm in replicating the experimental data.

Table C1. The isotherm performance of the Plutonium data.

Pu	r^2	Akaike #	Score	Ranking	# Parameters	# Operations	Variance
Dubinin-Astashov	0.72	66.24111	5	1	3	10	9.09
Langmuir Uniform Distribution	0.69	69.06384	8	2	3	6	10.13
Khan	0.69	69.08955	9	3	3	12	10.14
Langmuir	0.69	69.1409	10	4	3	6	10.16
Competive Quadratic with U	0.69	69.19214	12	5	3	6	10.18
FG-JF	0.752	70.56626	15	6	6	13	8.07
FG-LF	0.687	69.16653	15	6	3	6	10.17
SRS	0.687	69.21772	17	8	3	6	10.19
Jaroniec-Marczweski	0.687	69.21772	17	8	3	10	10.19
Langmuir-Freunlich	0.678	67.62537	18	10	2	2	10.47
BET	0.679	69.92407	23	11	3	8	10.47
Bubinin-Radushevik	0.679	69.92407	23	11	3	6	10.47

Myers	0.679	72.30791	27	13	4	10	10.47
Redlich-Peterson	0.685	-103.932	30	14	5	13	0.011
Radke-Prausnitz	0.616	72.24317	32	15	2	4	12.5
Toth	0.617	-103.646	35	16	3	5	0.0134
General-Y	0.67	-105.021	36	17	4	14	0.0116
Volmer	0.585	-99.3871	38	18	4	11	0.0144
Temkin	0.46	81.23325	38	18	2	5	17.65
IAST	0.616	-105.945	39	20	2	10	0.0134
Jovanovic	0.616	-105.945	39	20	2	2	0.0134

Table C2. The performance of the various models of the Np data.

Isotherm	Parameter	# operation	Variance	Akaike	r^2
Multicomponent Freundlich	4	7	488065	636.3095	0.42
Dubinin-Radushekiv	4	7	450808	632.516	0.39
Radke-Prausdnik	3	6	452480	630.4969	0.39
Relich-Peterson	5	9	108413	566.6745	0.97
Toth	3	6	421	297.052	0.18
Myers	3	5	40191	514.8351	0.55
Temkim	2	4	393188	621.6324	0.34
IAST	4	11	27619	499.1098	0.38
Volmer	2	11	41058	513.7002	0.56
General-Y	5	13	29703	504.8236	0.4
Jovanovic	2	4	400532	622.5165	0.4
Jaroniec	3	7	462956	631.5903	0.35

Table C3. The isotherm performance of the strontium data.

Sr	**r^2**	**Akaike #**	**Score**	**Ranking**	# Parameters	# Operations	Variance
Dubinin-Astashov	0.975	141	8	2	3	10	45.9
Langmuir Uniform Distribution	0.965	154	20	8	3	12	65.5
Khan	0.9655	153	15	5	3	6	64.67
Langmuir	0.9655	154	17	6	3	6	65.23
Competive Quadratic with U	0.979	144	7	1	6	13	39.99
FG-JF	0.96	-246	33	19	4	11	0.00062

Table C3. The isotherm performance of the strontium data.

Sr	r^2	Akaike #	Score	Ranking	# Parameters	# Operations	Variance
FG-LF	0.965	-251	30	16	4	14	0.00054
SRS	0.96	157	30	16	2	2	76
Jaroniec-Marczweski	0.962	159	29	15	4	10	70.5
Langmuir-Freunlich	0.967	152	11	3	3	6	61.96
BET	0.965	154	18	7	3	10	65.2
Bubinin-Radushevik	0.962	156	26	13	3	8	70.5
Myers	0.977	-267	25	11	3	5	0.00036
Redlich-Peterson	0.967	152	11	3	3	6	61.96
Radke-Prausnitz	0.962	156	25	11	3	6	70.48
Toth	0.96	158	31	18	3	6	74.25
General-Y	0.98	-268	23	9	5	13	0.00031
Volmer	0.96	-250	35	20	2	10	0.00062
Temkin	0.431	249	39	21	2	5	1068
IAST	0.98	-270	24	10	2	2	0.00035
Jovanovic	0.96	156	27	14	2	4	74.24

Table C4. The isotherm performance of the uranium data.

Uranium	r^2	Akaike	Score	Ranking	# Parameters	# Operations	Variance
Dubinin-Astashov	0.77	489	21	9	3	10	25894
Langmuir Uniform Distribution	0.31	566	41	20	3	12	131598
Khan	0.776	513	24	14	3	6	42652
Langmuir	0.23	574	44	21	3	6	155345

Table C4. The isotherm performance of the uranium data.

Uranium	r^2	Akaike	Score	Ranking	# Parameters	# Operations	Variance
Competive Quadratic with Np	0.86	497	11	1	6	13	26242
FG-JF	0.72	454	23	12	4	11	11622
FG-LF	0.7	458	26	16	4	14	12676
SRS	0.776	511	23	12	2	2	42742
Jaroniec-Marczweski	0.814	507	18	6	4	10	35475
Langmuir-Freunlich	0.827	501	13	2	3	6	33018
BET	0.82	503	15	3	3	10	34327
Bubinin-Radushevik	0.776	513	26	16	3	8	42742
Myers	0.745	448	17	4	3	5	10755
Redlich-Peterson	0.776	513	25	15	3	6	42740
Radke-Prausnitz	0.776	513	26	16	3	6	42742
Toth	0.8	508	21	9	3	6	38485
General-Y	0.74	453	20	8	5	13	10988
Volmer	0.74	447	17	4	2	10	10981
Temkin	0.31	564	40	19	2	5	131846
IAST	0.71	452	22	11	2	2	12246
Jovanovic	0.81	504	18	6	2	4	36626

Appendix D

The sensitivity plots of the DA model predictions for the Pu sorption data is shown in Figure D1.

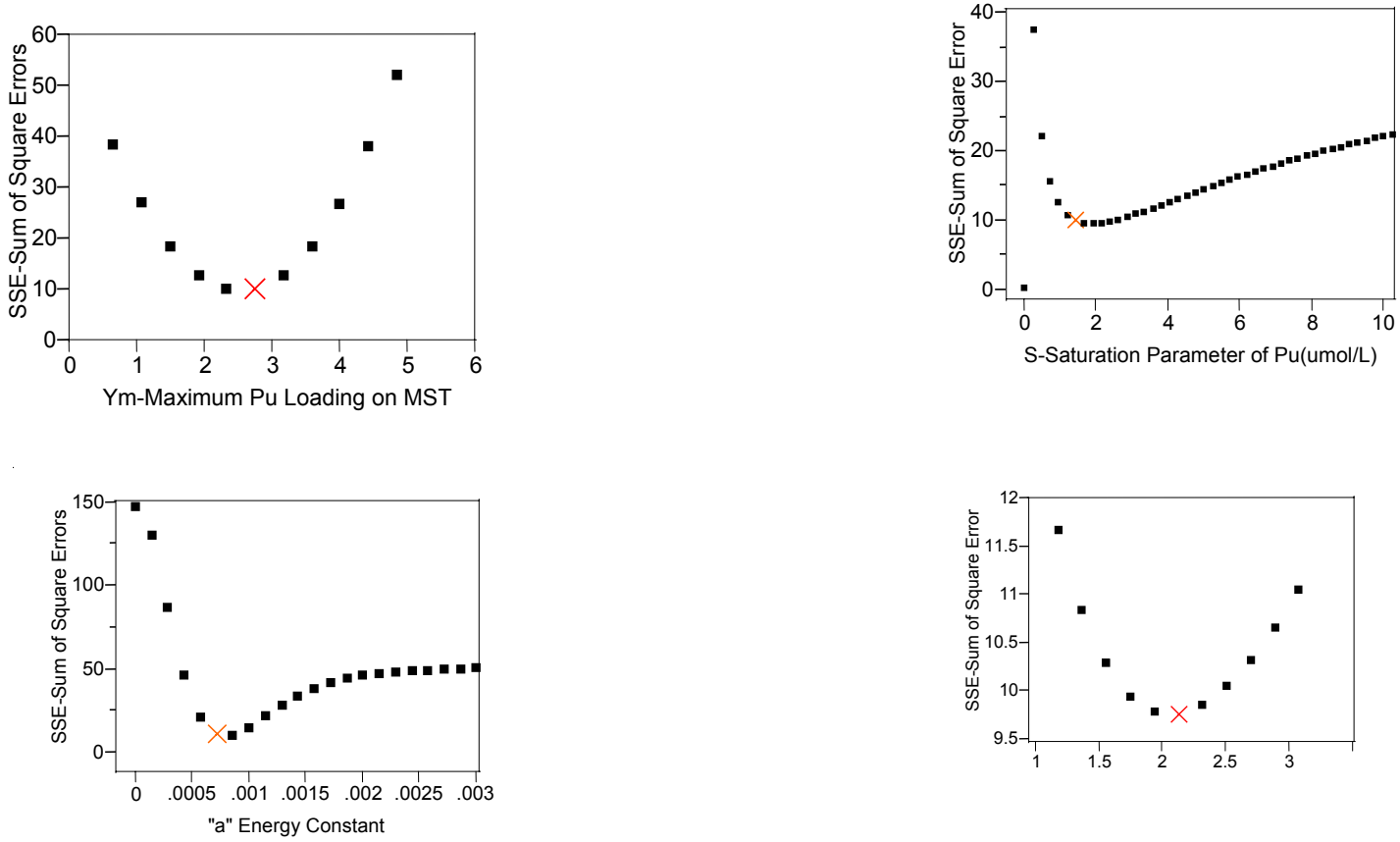

Figure D1. Sensitivity plots of the Dubinin-Astashov parameters determined from the Pu data at 25 ºC .

In Figure D1, the ordinate variable is the Sum of Squares of the Error (SSE). Recall that SSE is the deviation or distance between the model at current parameter values and the data. In the four graphs shown in Figure D1, we changed only one variable at a time (shown in the coordinate scale) while keeping the other variables at the optimized values. Inspection of Figure D1 reveals the most sensitivity parameters – see Appendix A – are "Y_m" (maximum loading, the pre-exponential term in the equation above) and the value "a", associated with the specific adsorption energy of the sites on MST. The parameter "a" is equivalent to the parameter "E" mentioned earlier. A significant increase in the SSE values with small changes in the "Y_m" and "a" occurs. In Figure D1, the optimal parameter is at the minimum value of SSE. For example, looking at the SSE versus "n" sub-figure the data point marked with a red "X" symbol is the value of "n" used in the Pu isotherm equation.

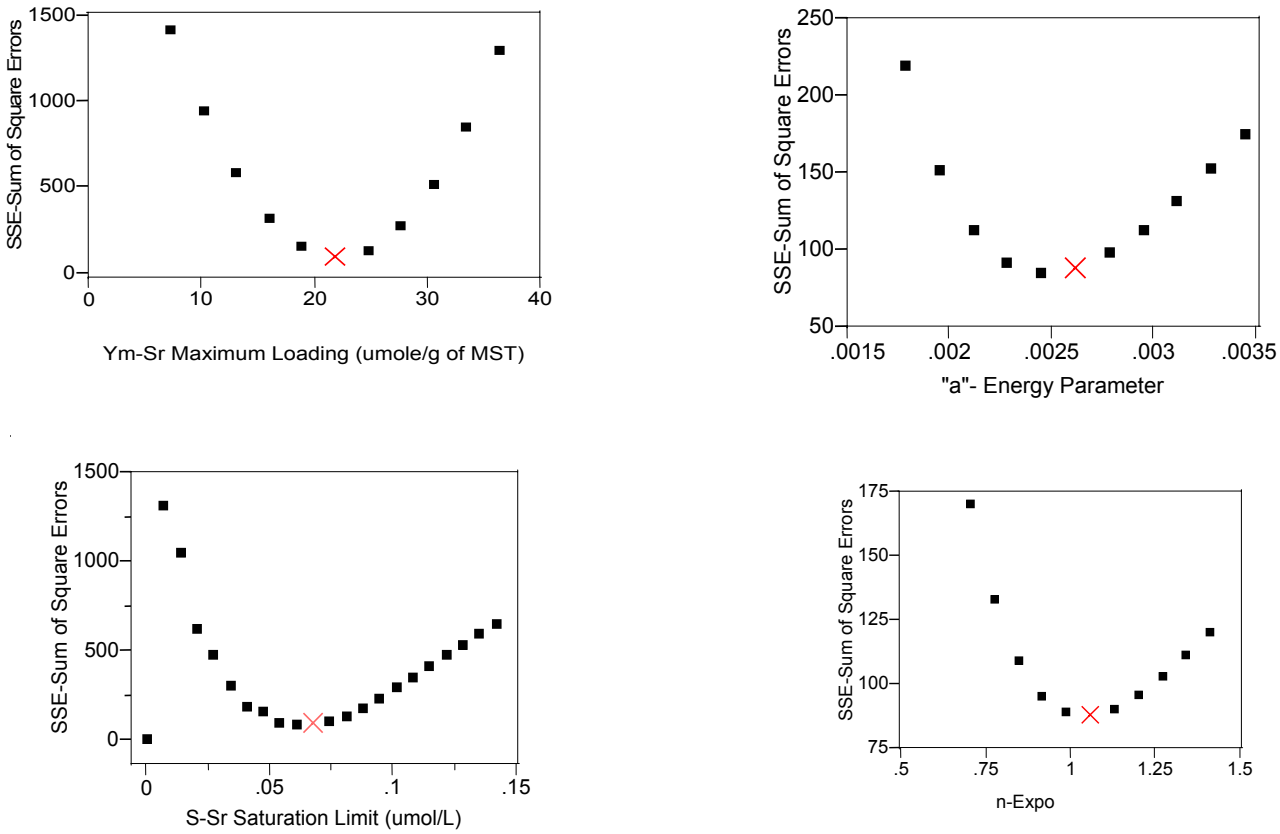

Figure D2. The sensitivity graphs of the Dubinin-Astashov model for the Sr loading data (at 25 ºC).

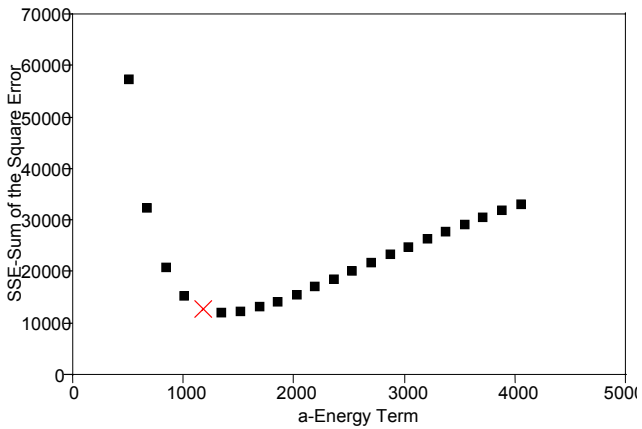

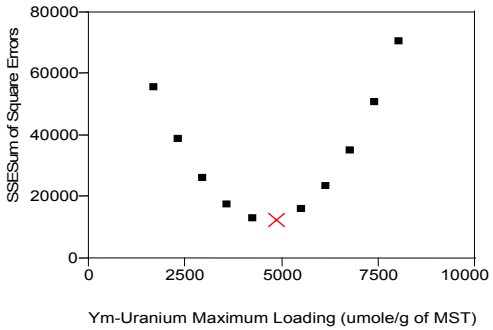

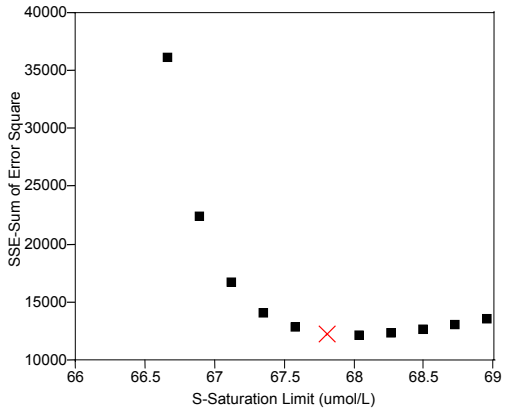

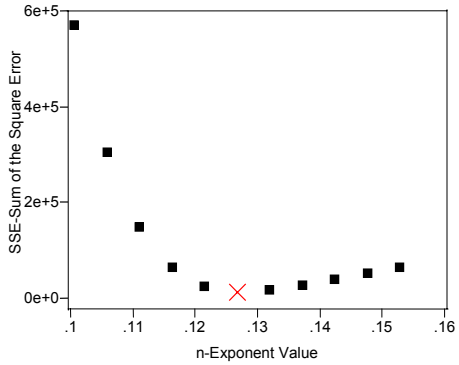

Figure D3. Sensitivity plots of the Dubinin-Astashov isotherm for uranium.

Appendix E

The Pu, Sr, U and Np sorption after 24 hours are shown in Figures E1, E2, E3 and E4. Except for Figure E4, the figures include the model prediction as well as the 95% prediction confidence curve.

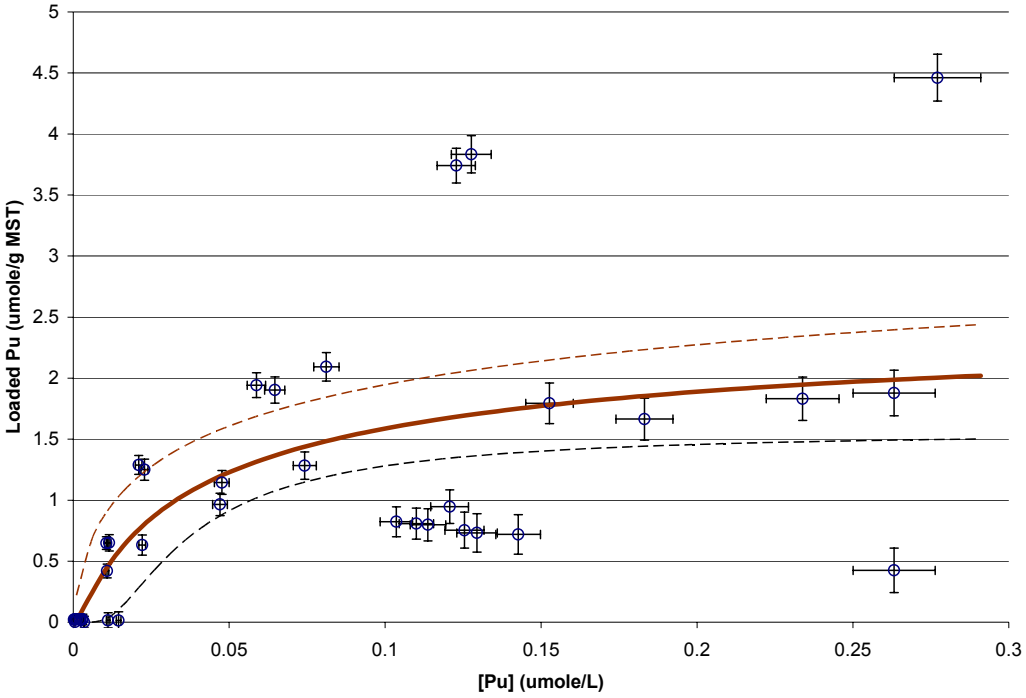

Figure E1. The Pu sorption data after 24 hours of testing.

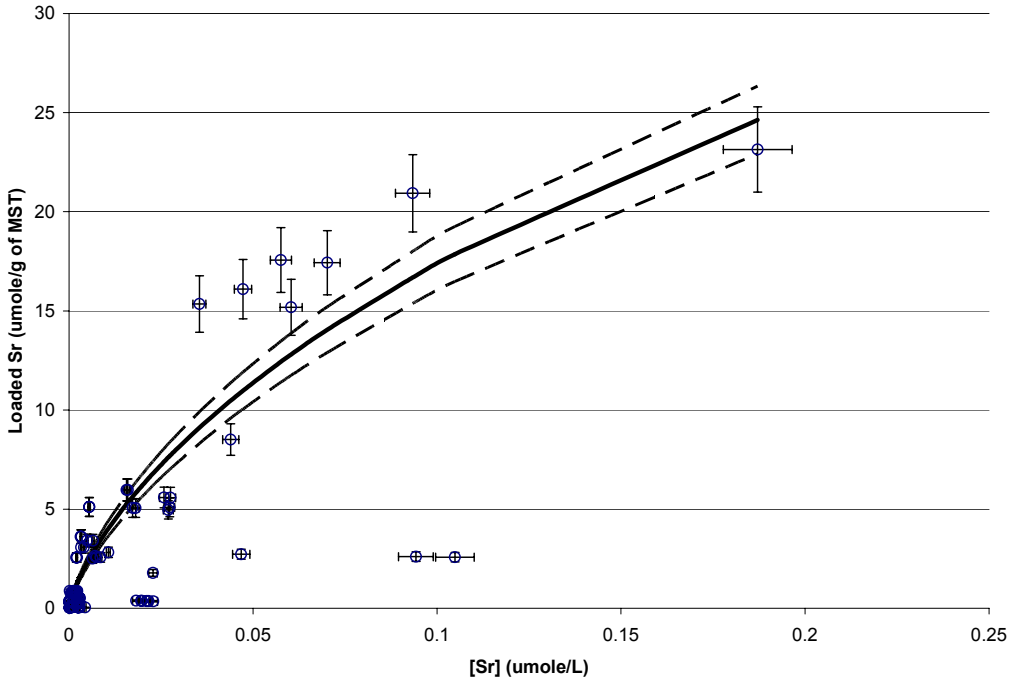

Figure E2. The Sr sorption data after 24 hours of testing.

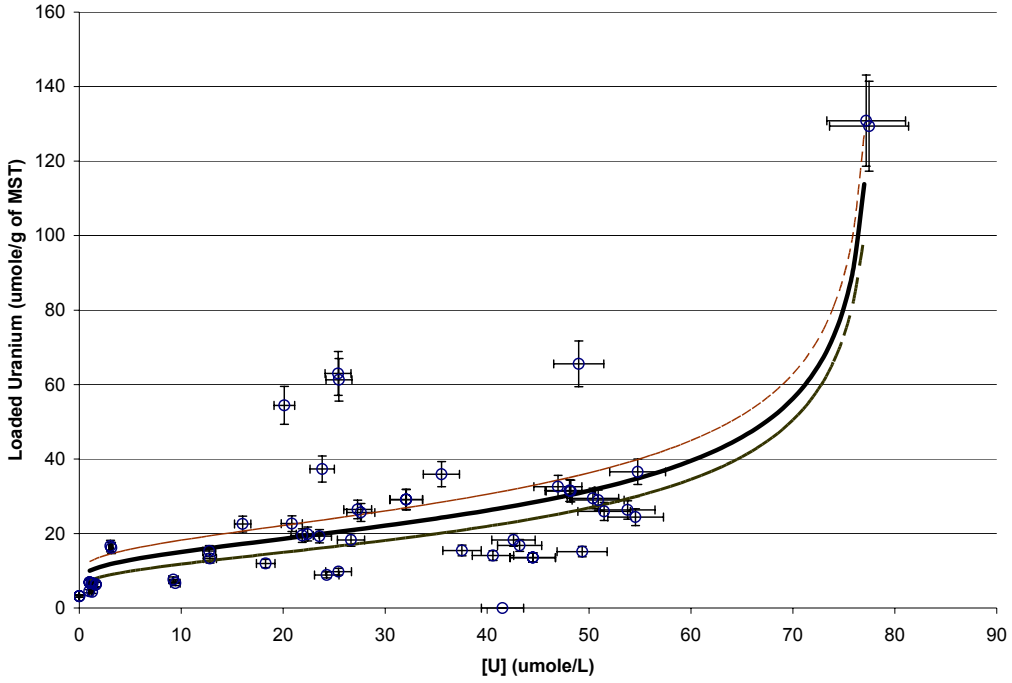

Figure E3. The Uranium Sorption data after 24 hours of testing.

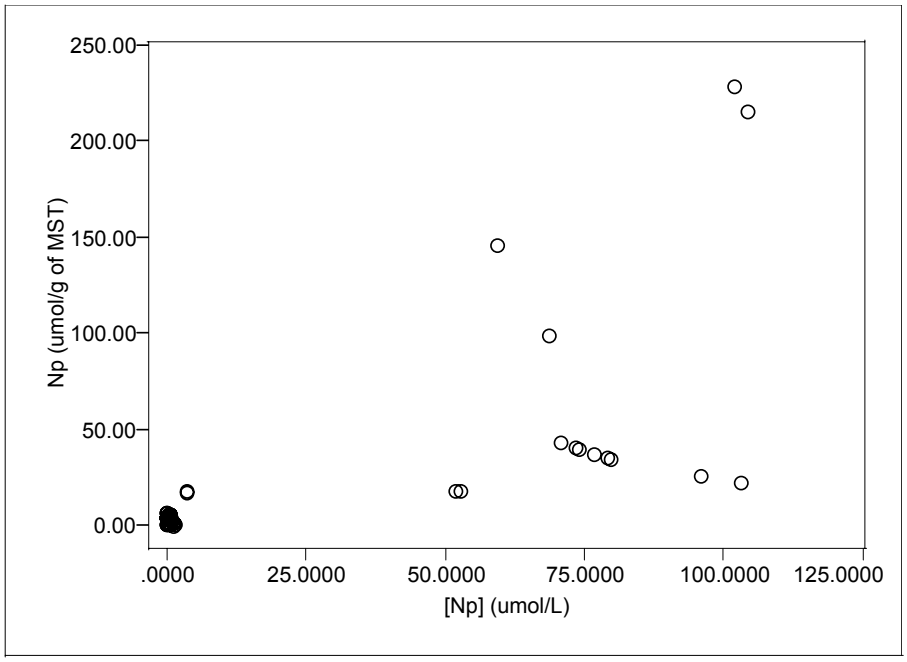

Figure E4. The Np sorption data at 25 ºC.

Appendix F

A summary of the Dubinin-Astashov equations for the four radionuclides are shown in Table F1.

Table F1. A summary of the Dubinin-Astashov parameters found for the radionuclides. Note the fitting with the Np data at 25 ºC was poor. No successful fitting was possible with the Np data at three different temperatures.

Component	Maximum Loading (umole/g of MST)	Pre-temperature coefficient "a"	Saturation Limit (umol/L)	Exponent Value	Calculated Adsorption Energy (J/mole)
Pu-25ºC	2.6±0.5	8.7±6.3E-4	0.83±1.2	2.1±1.5	238
Pu-25,45 & 65ºC	471±173	0.27±0.14	3.6±9.2	0.41±0.02	202
Sr-25ºC	23±25	2.5±0.9E-3	0.07±0.12	1.1±0.28	1929
Sr-25, 45 &65ºC	410±138	0.09±0.02	0.42±0.11	0.55±0.01	662
U-25ºC	4845±1266	1248±1118*	67.8±0.46	0.126±0.01	2E-10
U-25, 45 & 65ºC	1866±472	20±15*	68±0.3	0.16±0.008	6E-8
Np-25ºC	65±9	0.001±0.0006	75.3±0.01	1.1±0.5	4437

References:

[1] M. C. Duff, D. B. Hunter, D. T. Hobbs, and S. D. Fink, "Characterization of Sorbed Strontium on Monosodium Titanate," WSRC-TR-2001-00245, June 21, 2001.
[2] M. C. Duff, D. B. Hunter. D. T. Hobbs, M. J. Barnes, and S. D. Fink, "Characterization of Sorbed Actinides on Monosodium Titanate," WSRC-TR-2001-00467, September 27, 2001.
[3] N. L. Dietz, J. A. Fortner, Z. Dai, J. P. Bradley, M. C. Duff, D. T. Hobbs, and S. D. Fink, "Transmission Electron Microscopy Analysis of Strontium and Actinide-Bearing Monosodium Titanate and Permanganate Treatment Solid," WSRC-TR-2002-00363, August 26, 2002.
[4] I. Langmuir, "The Adsorption of Gases on Plane Surfaces of Glass, Mica and Platinum," J. Am. Chem. Soc. Vol. 40 (1918), p. 1361.
[5] J. A. V. Butler and C. Ockrent, "Studies in Electrocapillarity. Part III. The Surface Tensions of Solutions Containing Two Surface Containing Two Surface Containing Two Surface-Active Solutes," J. Phys. Chem. Vol. 34(1930), pp. 2841-2845.
[6] H. M. Freundlich, J. Phys. Chem. Vol. 57(1906), pp. 385-470.
[7] M. M. Dubinin and L. V. Radushkevich, "Equation of the Characteristic Curve of Activated Charcoal," Chem. Zentr Vol. 1(1947), p. 875.
[8] M. M. Dubinin and L. V. Radushkevich, "Evaluation of Microporous materials with a New Isotherm," Dokl. Akad. Nauk SSSR, Vol. 55(1966), p. 331.
[9] M. M. Dubinin and V. A. Astakhov, "2nd Int. Conf. On Molecular-Sieving Zeolites," (1970).
[10] M. J. Tempkin and V. Pyzhev, "Recent modifications to Langmuir Isotherms," Acta Physiochim USSR, Vol. 12(1940), p. 217.
[11] D. M. Ruthven, "Principles of Adsorption and Adsorption Processes," J. Wiley, New York, 1984.
[12] R. R. Rounsley, "Benzene Adsorption on Activated Carbon," AIChE J. Vol. 7(1961), p. 308.
[13] R. H. Fowler and E. A. Guggenheim, "Statistical Thermodynamics," MacMillan, New York, 1939, p. 430.
[14] K. Kaczmarski and D. Antos, "Calculation of Chromatographic Band Profiles with an Implicit Isotherm," J. of Chromatography A, Vol. 862(1999), pp. 1-16.
[15] A. N. Frumkin, "A multicomponent Isotherm for Gas Adsorption," Z. Phys. Chem. Vol. 116(1925), p. 466.
[16] O. Relich and D. L. Peterson, "A useful Adsorption Isotherm," J. Phys. Chem. Vol. 63(1959), p. 1024.
[17] J. Toth, "A Multicomponent Isotherm for Liquid Adsorption," Acta Chim. Acad. Sci. Hung., Vol. 69(1971), p. 311.
[18] M. D. LeVan and T. Vermeulen, "Binary Langmuir-like and Freundlich isotherms for ideal adsorbed solutions," J. Phys. Chem. Vol. 85(1981), pp. 3247-3250.
[19] S. Suwanayuen, and R. P. Danner, "A Gas Adsorption Isotherm Based on Vacancy Solution Theory," AIChE J. Vol. 26(1980), pp. 68-76.
[20] C. J. Radke and J. M. Prausnitz, "A New Adsorption Isotherm for Heterogeneous Surfaces," Ind. Eng. Chem. Fund., Vol. 4(1972), p. 445.
[21] A. Meghea, R. Mihalache, G. Bumbac and I. Constantinescu, "Recent developments in Isotherm Adsorption," Sci. Techn. Env. Protection, Vol. 3(1994), p. 10.

[22] N. G. Buckman, J. O. Hill, and R. J. Magee, "A New Adsorption Isotherm for Gases," Microchem. J., Vol. 28(1983), p. 470.
[23] G. Sposito, "Derivation of the Freundlich Equations for Ion Exchange Reactions in Soils," Soil Sci. Soc. Am. J. Vol. 44(1980), p. 652.
[24] M. Jaroniec and R. Madey, "Physical Adsorption on Heterogeneous Solids," Elsevier, Amsterdam, (1998).
[25] I. Quinones and G. Guiochon, "Isotherms for Liquid Adsorption Systems," J. Chromatogr. A, Vol. 15(1998), p. 796.
[26] M. Jaroniec and J. Toth, "Modifications to the Langmuir Isotherm: Extension to Multicomponent Adsorption Systems," J. Colloid Polym. Sci., Vol. 254(1976), p. 643.
[27] J. F. Porter, G. McKay, and K. H. Choy, "The Prediction of Sorption from a Binary Mixture of Acidic Dyes Using Single- and Mixed-isotherm Variants of the Ideal Adsorbed Solute Theory," Chemical Engineering Science, Vol. 54(1999), pp. 5863-5885.
[28] A. L. Myers and J. M. Prausnitz, "Thermodynamics of Mixed-gas Adsorption," AIChE J. Vol. 11(1965), pp. 121-127.
[29] C. J. Radke and J. M. Prausnitz, "Thermodynamics of Multi-solute Adsorption from Dilute Liquid Solution,"AIChE J. Vol. 18(1972), pp-761-768.
[30] C. Sheindorf, M. Rebhum and M. Sheintuch, "A Freundlich-type multicomponent isotherm," J. Colloid Interface Sci. Vol. 79(1981), pp. 136-142.
[31] D. T. Hobbs, M. G. Bronikowski, T. B. Edwards, and R. L. Pulmano, "Final Report of Phase III Testing of Mono-Na Titanate Adsorption Kinetics," WSRC-TR-99-00134, Rev. 0, May 28,, 1999.
[32] D. T. Hobbs, and R. L. Pulmano, "Phase IV Simulant Testing of Mono-Na Titanate Adsorption Kinetics", WSRC-TR-99-00219, Rev. 0, June 29, 1999.
[33] D. T. Hobbs, "Phase V Simulant Testing of Monosodium Titanate Adsorption", WSRC-TR-2000-00142, Rev. 0, May 22, 2000.
[34] D. T. Hobbs, "Solution Composition and Alternate Materials," WSRC-TR-2001-00436, August, 2001.
[35] D. T. Hobbs and S. D. Fleichman, "Fissile Solubility and MST Loading Test," WSRC-RP-92-1273, March 29, 1992.
[36] A. McQuarrie, R. Shumway, and C. L. Tsai, "The Model Selection Criterion AICu," Statistics & Probability Letters 34(1997) PP 285-292.
[37] G. Atun and Z. Kaplan, "Influences of Salt Concentration, Loading and pH on Strontium Adsorption," Journal of Radioanalytical and Nuclear Chemistry, Articles, Vol. 211, No 2 (1996), pp. 425-434.
[38] P. Jandera, Z. Posvec and P. Vraspir, "Mobile Phase Effects on Single-Component and Competitive Adsorption Isotherms in Reversed-Phase Systems," J. of Chromatography A, 734 (1996), PP 125-136.
[39] A. Meghea, H. H. Rehner, I. Peleanu, and R. Mihalache, "Test-fitting on Adsorption Isotherms of Organic Pollutants from Waste Waters on Activated Carbon," J. of RadioAnalytical and Nuclear Chemistry, 229 (1998), PP 105-110.
[40] S. Al-Asheh, F. Banat, R. Al-Omari, and Z. Duvnjak, "Predictions of Binary Sorption Isotherms for the Sorption of Heavy Metals by Pine Bark Using Single Isotherm Data," Chemosphere 41(2000), PP 659-665.
[41] M. M. Dubinin, and V. A. Asthasov, "A New Modified DA Isotherm Equation," Izvest. Akad. Nauk. SSSR (ser. Khim.), 11(1971), p 4.

[42] C. Wittrock, H. H. Kohler, and J. Seidel, "A Multilayer Adsorption Isotherm for Solutions," Langmuir, 12(1996) p. 5550.
[43] I. Quinones, and G. Guiochon, "Application of Different Isotherm Models to the Description, of Single-Component and Competitive Adsorption Data," J. of Chromatography A, 734(1996), PP 83-96.
[44] D. P. Valenzuela and A. L. Myers, "Adsorption Equilibrium Data Handbook," Prentice Hall, New Jersey, 1989.
[45] A. R. Khan, I. R. Al-Waheab and A. Al-Haddad, "A Generalized Equation for Adsorption Isotherms for Multi-Component Organic Pollutants in Dilute Aqueous Solutions," Environ. Tech. 17 (1996), PP. 13-23.
[46] A. R. Khan, M. R. Riazi and Y. A. Al-Roomi, " A Thermodynamic Model for Liquid Adsorption Isotherms," Separation and Purification, Techn. 18(2000), PP 237-250.
[47] M. Jaroniec and A. W. Marcewski, " A generalized Isotherm Model for Liquid Adsorption," Monatsh. Chem., 115(1984), p. 541.
[48] R. H. Fowler and E. A. Gugenheim, "Statistical Thermodynamics," MacMillan, NY 1939, p 430.